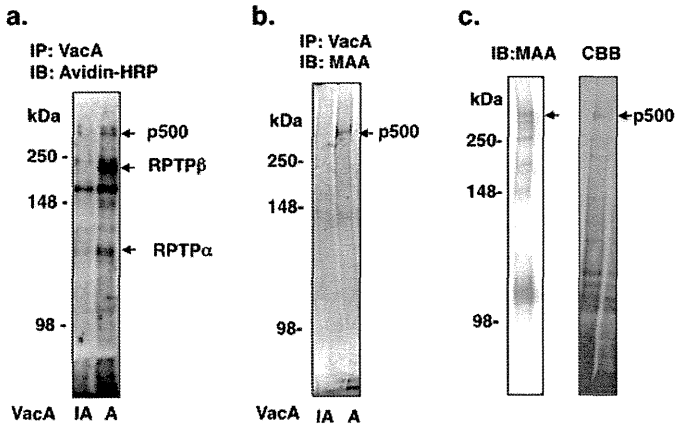

FIGURE 1. **Purification of p500 from AZ-521 cells by MAA-agarose column.** *a*, after biotinylation of surface proteins, AZ-521 cells were solubilized and immunoprecipitated with heat-inactivated (*IA*) or wild-type VacA (*A*) as described under "Experimental Procedures." Immunocomplexes were separated by SDS-PAGE in 6% gels and transferred to PVDF membranes. VacA-binding proteins were detected with streptavidin-HRP. *b*, proteins immunoprecipitated (*IP*) with heat-inactivated or wild-type VacA were separated by SDS-PAGE in 6% gels and transferred to PVDF membranes, which were incubated with MAA-lectin conjugated to digoxigenin and then with anti-digoxigenin Fab fragments conjugated to alkaline phosphatase, followed by reaction with 4-nitro blue tetrazolium chloride/5-bromo-4-chloro-3-indolyl phosphate. *c*, biotinylated AZ-521 cell lysates were incubated overnight with a MAA-agarose column (2 ml bed volume), which was washed with 20 ml of Sol buffer. Bound proteins were eluted, concentrated, and separated by SDS-PAGE as described under "Experimental Procedures." MAA-lectin blotting is shown in the *left panel* and Coomassie Brilliant Blue (*CBB*) staining in the *right panel*. The stained p500 protein band was hydrolyzed with trypsin and subjected to LC-MS/MS analysis. The procedures described in *a*-c were repeated at least three times with similar results. *IB*, immunoblot.

VacA Induced Formation of Autophagosomes and Autolysosomes in AZ-521 Cells—To determine whether VacA induces autophagic vacuoles, AZ-521 cells were incubated with 120 nM VacA. We microscopically observed that active VacA (A) is sufficient to trigger autophagic vacuoles such as autophagosomes containing LC3-II after a 4-h incubation, followed after by 12 h incubation by formation of autolysosomes as detected by LysoTracker (Fig. 4*A*). Cells incubated with heat-inactivated VacA (IA) showed low or undetectable levels of these autophagic vacuoles after 12 h incubation. Furthermore, confocal microscopy analysis showed that intracellular VacA partially co-localized with LC3-II and LRP1, consistent with the conclusion that LRP1 plays an important role in VacA-induced autophagosome formation. However, LRP1 knockdown with siRNA suppressed VacA co-localization with LC3-II, suggesting that LRP1 is essential for formation of autophagosomes in response to VacA (Fig. 4*B*).

Vacuoles Caused by VacA Are Characterized as Autophagosomes and Autophagolysosomes—Confocal microscope visualization of LC3-II, VacA, and LRP1 revealed that vacuoles caused by VacA are of at least two different types; one type consists of autophagic vacuoles such as autophagosomes and autophagolysosomes and the second type lacks LC3-II (Fig. 5*A*). These observations support previous findings that VacA-dependent autophagosomes and large vacuoles are distinct intracellular compartments and autophagy is independent of the formation of large vacuoles by VacA (29). Interestingly, some vacuoles observed with RPTPβ revealed small light vacuoles without LC3-II (Fig. 5*B*) and dense vacuoles with RPTPα were devoid of LC3-II (Fig. 5*C*). Although little is known about the physiological importance of the autophagy-dependent degradation of mitochondria (mitophagy) (39), several studies have suggested that PINK1/parkin-dependent mitophagy selectively degrades mitochondria (40), implying that mitophagy contributes to mitochondrial quality control. As shown in Fig. 5*D*, after 10 h incubation mitochondria were not observed in vacuoles with LC3-II. Furthermore, recent studies revealed that p62 binds to LC3 on the autophagosome membrane to target aggregates to autophagosomes for degradation (41). After 24 h incubation, VacA, not heat-inactivated VacA, induced formation of puncta, which were colocalized with LC3-II and p62 (Fig. 5*E*).

Among VacA-binding Proteins, LRP1, but Not RPTPs and FN, Mediates VacA-dependent Autophagy—To assess which VacA-binding proteins were responsible for VacA-induced autophagy, we examined the effect of silencing and knockout of the genes for RPTPβ, RPTPα, and fibronectin. Although LRP1 silencing blocked VacA-stimulated generation of LC3-II as shown in Fig. 3*b*, silencing these other genes did not show a similar effect, suggesting that only LRP1 may be critical for VacA-induced autophagy (Fig. 6).

LRP-1, but Not RPTPs, Mediates Cleavage of Caspase-7 and PARP Caused by VacA—Excessive autophagy can cause cell death (34, 42). Furthermore, VacA-induced cell death may occur through a programmed necrosis pathway in a caspase-independent process in AZ-521 cells (27). Therefore, we examined whether VacA-induced cell death resulted from autophagy via an LRP1-dependent pathway. Western blot analysis showed that LRP1 silencing blocked VacA-induced generation of LC3-II as well as cleavages of effector caspase-7 and PARP, suggesting that VacA binding to LRP-1 is responsible for not only autophagy but also for apoptosis in AZ-521 cells (Fig. 7).

Effects of Atg5 Silencing, Z-VAD-fmk and Necrostatin-1 on VacA-induced LC3-II Production and Cleavage of PARP—To further examine the link between autophagy and apoptosis, the effects of Atg5 silencing with siRNA, general caspase inhibitor (Z-VAD-fmk) and RIPK inhibitor (Necrostatin-1) on LC3-II generation, and PARP cleavage was evaluated. Silencing of the *Atg5* gene inhibited generation of LC3-II as well as PARP cleavages in response to VacA (Fig. 8), whereas both inhibitors, Z-VAD-fmk and Necrostatin-1, which interfere with apoptosis (43), did not inhibit VacA-induced autophagy, suggesting that VacA-induced autophagy precedes apoptosis in AZ-521 cells. Necrostatin-1, which inhibits necroptosis (44), did not interfere with VacA-induced generation of LC3-II and PARP cleavage.

Effect of Anion Channel Blockers, NPPB and DIDS, on VacA-induced LC3-II Production—To assess whether membrane channels formed by VacA may also be involved in autophagy (29), we tested the effects of pretreating AZ-521 or AGS cells with chloride channel blockers, NPPB and DIDS, which are known to block both VacA-mediated channel activity and cellular vacuolation (45). AZ-521 cells were pretreated for 30 min with 100 μM NPPB or 100 μM DIDS prior to incubation with VacA for 6 h. Both NPPB and DIDS inhibited VacA-induced LC3-II generation in AZ-521 cells (Fig. 9*a*), but not in AGS cells under these conditions (Fig. 9*b*).

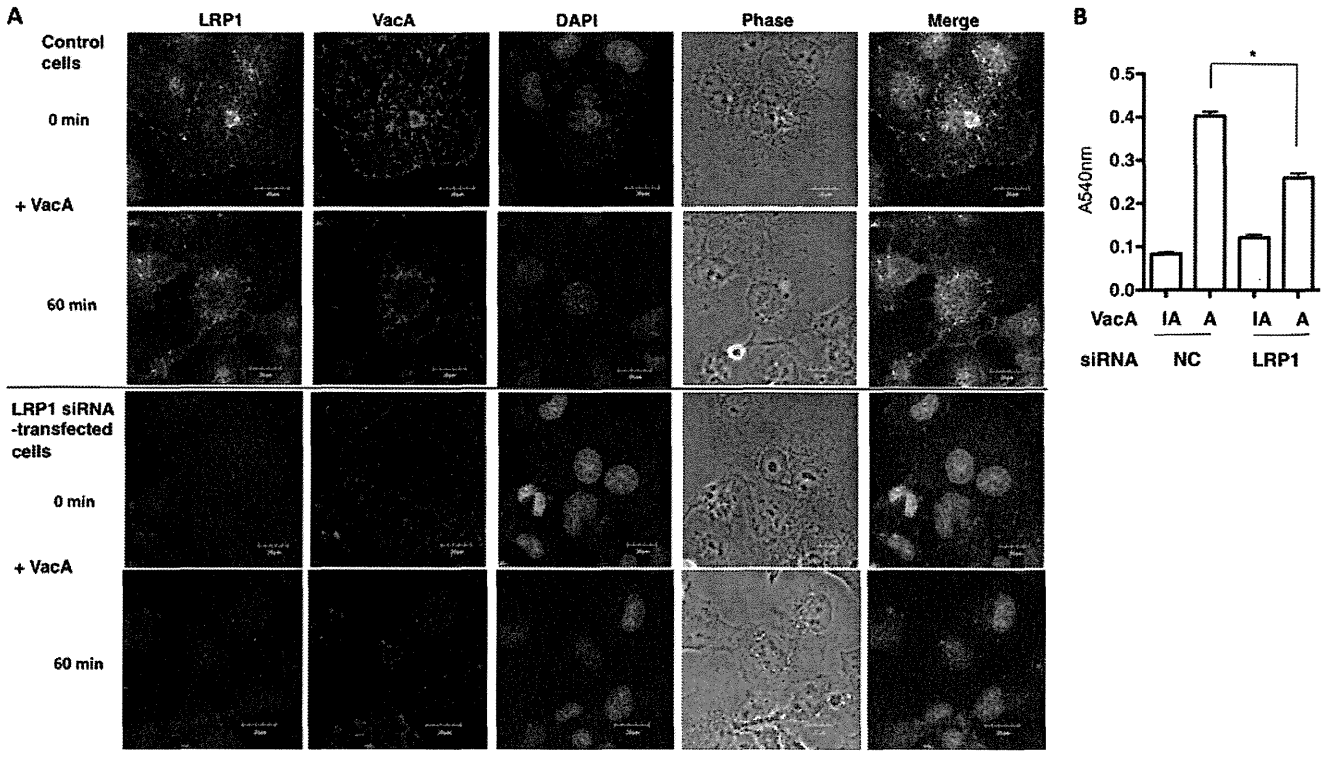

FIGURE 2. **LRP1-dependent VacA internalization and vacuolation in AZ-521 cells.** *A*, confocal microscopic analysis of VacA binding to AZ-521 cells via LRP1. Nontargeting (*NC*) or LRP1 siRNA-transfected AZ-521 cells were incubated with Alexa 555-labeled VacA (*red*) for 30 min at 4 °C or for 1 h at 37 °C, fixed with 4% paraformaldehyde, and reacted with anti-LRP1 antibodies (*green*) as described under "Experimental Procedures." The nuclei were stained with DAPI. A merged picture shows co-localization of VacA and LRP1 in AZ-521 cells. *Bars* represent 20 μm. Experiments were repeated two times with similar results. *B*, silencing of LRP1 gene inhibited VacA-induced vacuolation. The indicated siRNA-transfected AZ-521 cells were incubated with 120 nM heat-inactivated (*IA*) or wild-type VacA (*A*) for 18 h at 37 °C. Vacuolating activity was evaluated by neutral red uptake assay as described under "Experimental Procedures." Data are presented as mean ± S.D. and significance is (*) $p < 0.01$ ($n = 3$). Experiments were repeated three times with similar results.

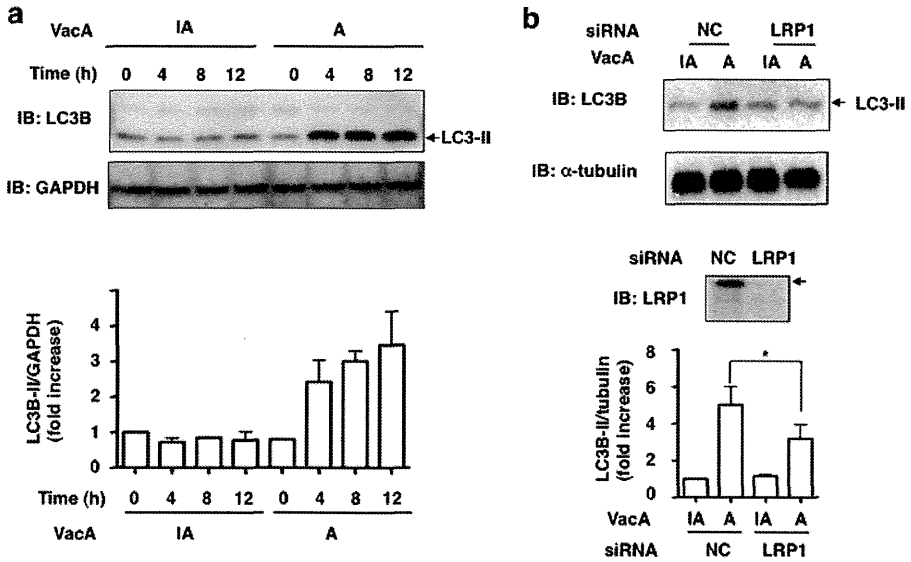

FIGURE 3. **VacA induced generation of LC3-II in an LRP1-dependent manner.** *a*, AZ-521 cells were incubated with 120 nM heat-inactivated (*IA*) or wild-type VacA (*A*) for the indicated time points and harvested for immunoblotting (*IB*) with the indicated antibodies. Quantification of VacA-induced LC3-II levels in AZ-521 cells was performed by densitometry (*bottom panel*). Data are presented as mean ± S.D. of values from two experiments. Experiments were repeated two times with similar results. *b*, the indicated siRNA-transfected AZ-521 cells were incubated with 120 nM heat-inactivated or wild-type VacA for 4–5 h at 37 °C and the cell lysates were subjected to immunoblotting with the indicated antibodies. α-Tubulin served as a loading control. Quantification of VacA-induced LC3-II levels in AZ-521 cells was performed by densitometry (*bottom panel*). Data are presented as mean ± S.D. and significance is (*) $p < 0.01$ ($n = 4$). Experiments were repeated four times with similar results.

DISCUSSION

VacA has two functional domains, an N-terminal 33.4-kDa domain (named p33, p34 or p37, comprising residues 1–311) and a C-terminal domain of 54.8 kDa (named p55 or p58, comprising residues 312–821) (10, 46, 47). Vacuolization of epithelial cells by VacA is strictly dependent on the formation of anion-selective membrane channels, which are targeted to late endosomes after internalization of the toxin (45, 48). The pore

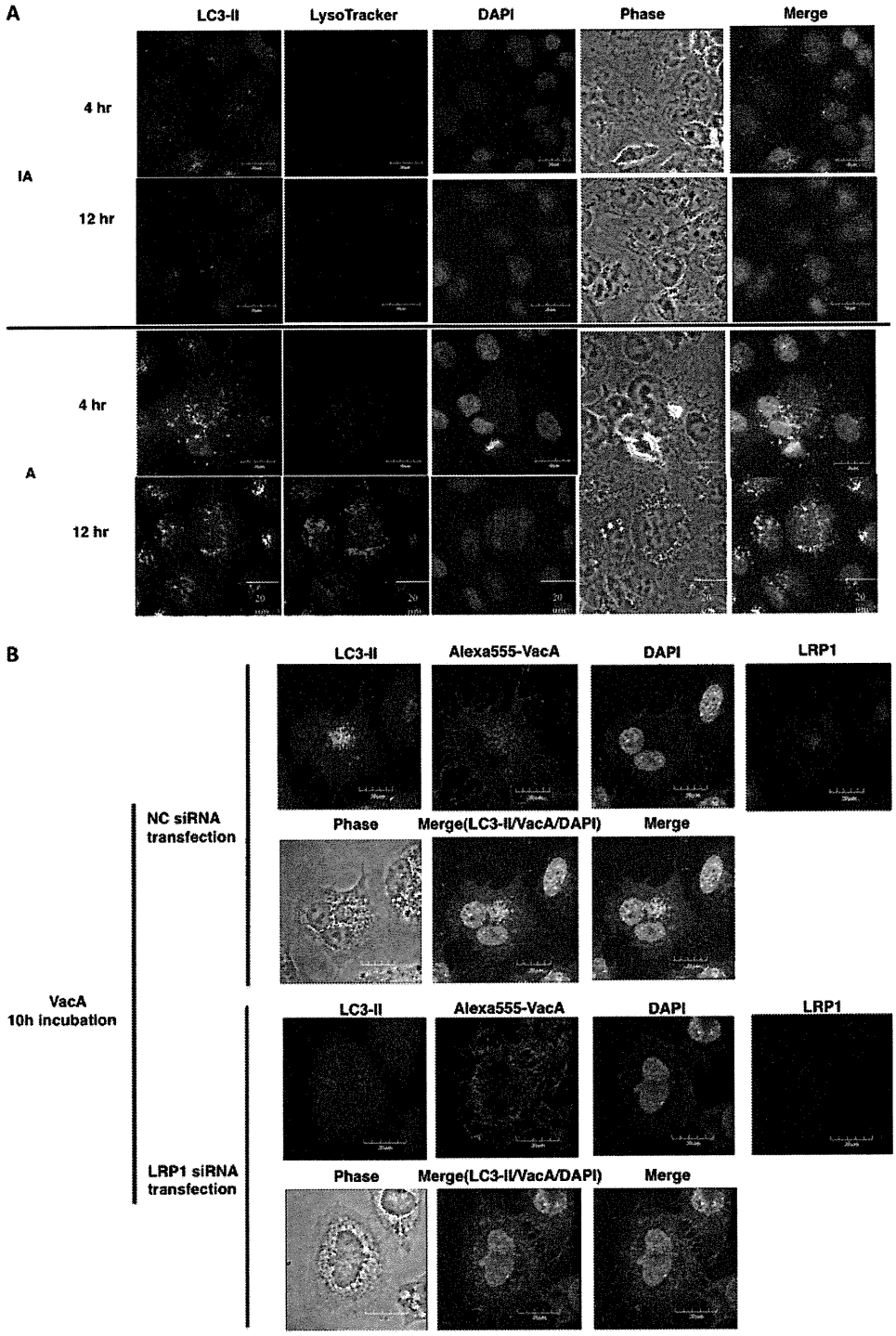

FIGURE 4. **VacA induced formation of autophagic vacuoles in AZ-521 cells via LRP1.** *A*, VacA-induced formation of autophagosomes and autolysosomes in AZ-521 cells. AZ-521 cells were incubated with 120 nM heat-inactivated (*IA*) or wild-type VacA (*A*) for the indicated time points and fixed for immunofluorescence staining with LC3B (*green*) antibodies as described under "Experimental Procedures." The acidic autophagolysosomes were stained by LysoTracker, as described under "Experimental Procedures." A merged picture shows co-localization in AZ-521 cells. The nuclei were stained with DAPI. *Bars* represent 20 μm. Experiments were repeated two times with similar results. *B*, induction of autophagy by VacA in an LRP1-dependent manner. The indicated siRNA-transfected AZ-521 cells were incubated with 120 nM Alexa 555-labeled VacA (*red*) for 10 h at 37 °C and fixed for immunofluorescence staining with anti-LC3B (*green*) or anti-LRP1 (*blue*) antibodies as described under "Experimental Procedures." A merged picture shows co-localization in AZ-521 cells. The nuclei were stained with DAPI. *Bars* represent 20 μm. Experiments were repeated two times with similar results.

and channel forming by the N-terminal p33 domain alone drives pleiotropic cellular activities of VacA; *i.e.* vacuolation, mitochondria damage, apoptosis (10, 47), autophagy (28, 29), and programmed necrosis (27), suggesting that VacA may be characterized as a pore-forming toxin (47). Another study has indicated that both p33 and p55 are required to form a functional channel in the inner mitochondria membrane and trigger apoptosis (49). In addition, it is now widely accepted that the C-terminal p55 domain of VacA plays an essential role in its binding to target cells (50, 51).

LRP1 Mediates VacA-induced Autophagy and Apoptosis

The present study defines a novel role for VacA signaling through LRP1 in AZ-521 cells, inducing autophagy and apoptosis (Fig. 7). LRP1 is a large endocytic receptor belonging to the LDL receptor family. This membrane protein consists of a 515-kDa heavy chain containing the extracellular ligand-binding domains and a noncovalently associated 85-kDa light chain, which consists of a transmembrane domain and a short cytoplasmic tail. LRP1 functions as a clearance receptor mediating

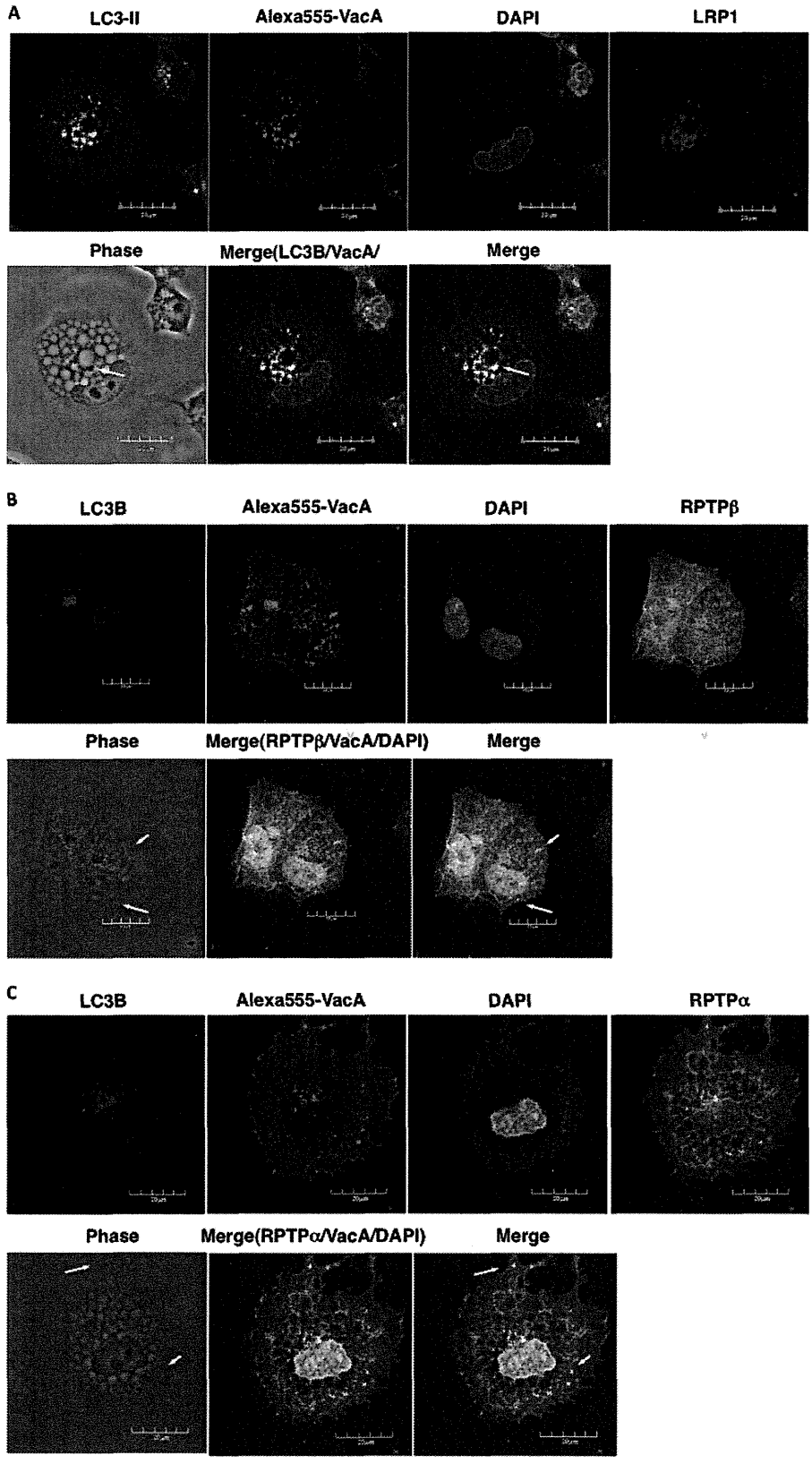

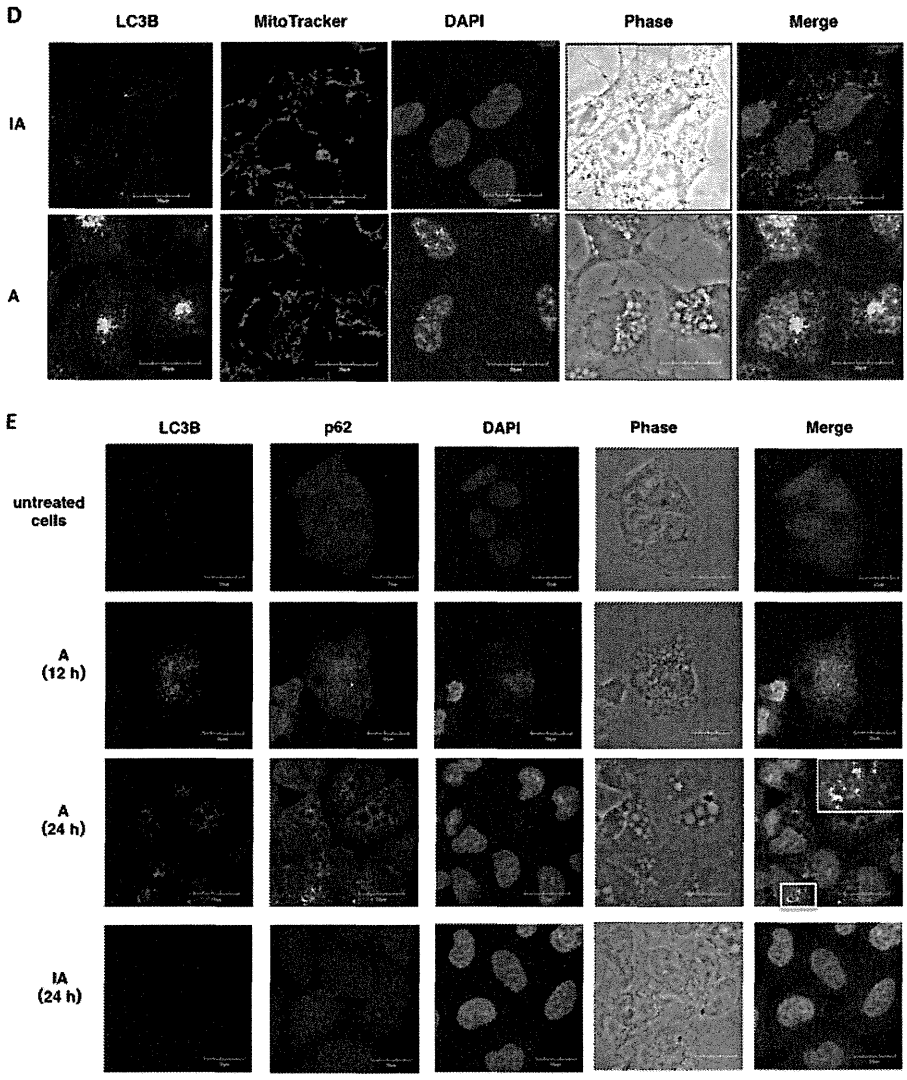

FIGURE 5—*continued*

the uptake and catabolism of various ligands from the pericellular environment, *e.g.* LRP1 binds to apolipoprotein E-rich lipoproteins, lipoprotein lipase, α_2-macroglobulin, lactoferrin, and tissue plasminogen activator; it functions in lipoprotein metabolism, degradation of proteases and proteinase/inhibitor complexes, activation of lysosomal enzymes and cellular entry of viruses, and bacterial toxin such as *Pseudomonas* exotoxin A (52). LRP1 has also been shown to function in the turnover of fibronectin (53).

This is the first study to provide evidence that LRP1 mediates autophagy. In AZ-521 cells, VacA triggered formation of autophagosomes, followed by autolysosome formation, consistent with the observations in AGS cells (29). Because LRP1 knockdown with siRNA resulted in inhibition of VacA-induced LC3-II generation and cleavage of both caspase 7 and PARP, induction by VacA of both autophagy and apoptosis occurred via, at least in part, association with LRP1. VacA also promoted formation of vacuoles containing RPTPβ and RPTPα, which

FIGURE 5. **Various vacuoles formed by VacA.** *A*, small autophagic vacuoles induced by VacA contain LC3-II, LRP1, and toxin: AZ-521 cells were incubated with 120 nM Alexa 555-labeled VacA (*red*) for 10 h at 37 °C and fixed for immunofluorescence staining with anti-LC3B (*green*), or anti-LRP1 (*blue*) antibodies or the nuclei were stained with DAPI as described under "Experimental Procedures." A merged picture shows co-localization in AZ-521 cells. *Solid arrows* show VacA, LC3B, and LRP1 colocalization to puncta. *Bars* represent 20 μm. Experiments were repeated two times with similar results. *B*, VacA-induced light vacuoles contain toxin and RPTPβ, and are different from autophagic vacuoles: AZ-521 cells were treated with 120 nM Alexa 555-labeled VacA (*red*) as similar to above. Cells were fixed and stained for anti-LC3B (*blue*), anti-RPTPβ (*green*), and with DAPI. A merged picture shows co-localization in AZ-521 cells. *Solid arrows* show VacA and RPTPβ colocalization to puncta. *Bars* represent 20 μm. Experiments were repeated two times with similar results. *C*, VacA-induced dense vacuoles contain toxin and RPTPα, and are different from autophagic vacuoles: AZ-521 cells were treated with 120 nM Alexa 555-labeled VacA (*red*) as similar to above. Cells were fixed and stained for anti-LC3B (*blue*), anti-RPTPα (*green*), and with DAPI. A merged picture shows co-localization in AZ-521 cells. *Solid arrows* show VacA and RPTPα colocalization to puncta. *Bars* represent 20 μm. Experiments were repeated two times with similar results. *D*, VacA-induced autophagic vacuoles do not contain functional mitochondria: AZ-521 cells were treated with 120 nM heat-inactivated (*IA*) or native VacA (*A*) for 10 h at 37 °C and 100 nM MitoTracker (*red*) was added to cells before fixation as described under "Experimental Procedures." Cells were stained for anti-LC3B (*green*), anti-p62 (*green*), and with DAPI. *Bars* represent 20 μm. Experiments were repeated two times with similar results. *E*, VacA induced p62 generation in a time-dependent manner. AZ-521 cells were treated with 120 nM heat-inactivated or native VacA for the indicated time points at 37 °C. Cells were fixed and stained for anti-LC3B (*red*) and with DAPI. Merged and higher magnification images of the outlined areas are shown. *Bars* represent 20 μm. Experiments were repeated two times with similar results.

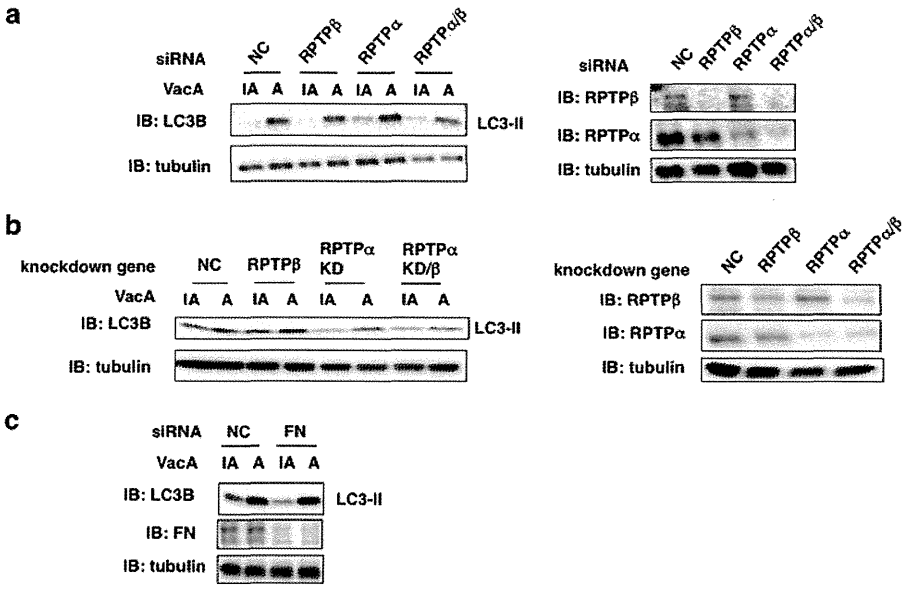

FIGURE 6. **Among VacA-binding proteins, LRP1, but not RPTPs and FN, mediates VacA-dependent autophagy.** *a*, the indicated siRNA-transfected AZ-521 cells were incubated with 120 nM heat-inactivated (*IA*) or wild-type VacA (*A*) for 4–5 h at 37 °C and the cell lysates were subjected to immunoblotting (*IB*) with the indicated antibodies. The knockdown levels of RPTPβ or RPTPα were detected by the antibodies (*right panel*). α-Tubulin served as a loading control. *b*, the indicated NC or RPTPβ siRNA-transfected AZ-521 cells were incubated with 120 nM heat-inactivated or wild-type VacA for 4–5 h at 37 °C and the cell lysates were subjected to immunoblotting with anti-LC3B or anti-FN antibodies. α-Tubulin served as a loading control. *c*, AZ-521 cells were transfected with NC or FN siRNA and treated with heat-inactivated or wild-type VacA for 4–5 h at 37 °C. Cell lysates were subjected to immunoblotting with the indicated antibodies. α-Tubulin served as a loading control. A blot representative of at least three separate experiments is shown.

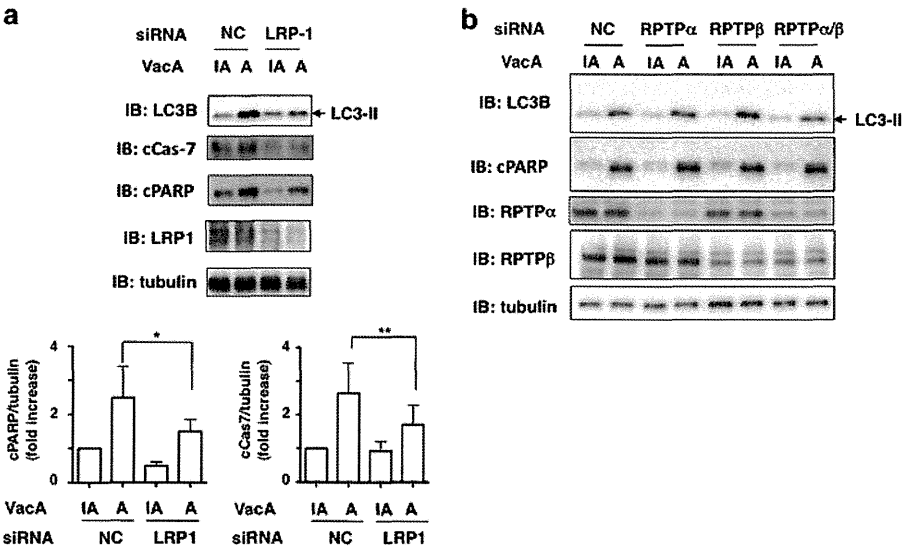

FIGURE 7. **LRP1, but not RPTPs, mediates VacA-dependent cleavage of caspase-7 and PARP.** *a*, NC or LRP1 siRNA-transfected AZ-521 cells were incubated with 120 nM heat-inactivated (*IA*) or wild-type VacA (*A*) for 6 h at 37 °C and the cell lysates were subjected to immunoblotting (*IB*) with anti-LC3B, anti-cleaved PARP, anti-cleaved caspase-7, or anti-LRP1 antibodies. α-Tubulin served as a loading control. A blot representative of four separate experiments is shown. Quantification of VacA-induced cleavage of PARP (*cPARP*) or caspase-7 (*cCas7*) levels in the indicated siRNA-transfected AZ-521 cells was performed by densitometry (*bottom panel*). Data are presented as mean ± S.D. and significance is (*) $p < 0.01$ ($n = 4$) and (**) $p < 0.03$ ($n = 4$). *b*, the indicated siRNA-transfected AZ-521 cells were incubated with 120 nM heat-inactivated or wild-type VacA for 6 h at 37 °C and the cell lysates were subjected to immunoblotting with anti-LC3B, anti-cleaved PARP, anti-RPTPα, or anti-RPTPβ antibodies. α-Tubulin served as a loading control. A blot representative of three separate experiments is shown.

were characterized as light and dense vacuoles, respectively, by confocal microscopy, and large vacuoles (Fig. 5). We observed the presence in AZ-521 cells of large vesicles without autophagosome markers in wild-type and Atg12 knockdown AGS cells (29). In general, vacuole formation caused by VacA is required for VacA channel activity (54). Our studies using chloride channel blockers, NPPB and DIDS, to address the relationship between VacA-induced autophagy and channel activity of VacA in AZ-521 cells treated with VacA revealed that these channel blockers inhibited LC3-II generation in response to VacA (Fig. 9), suggesting that channel activity may be required for LRP1-dependent autophagy. More interestingly, VacA-induced autophagy was not blocked by caspase inhibitor and RIPK inhibitor, suggesting that VacA-induced autophagy via LRP1 binding precedes apoptosis.

Autophagy is a degradation process that involves formation of autophagosomes, which engulf cytoplasmic components, and fuse with the lysosome/vacuole for degradation of con-

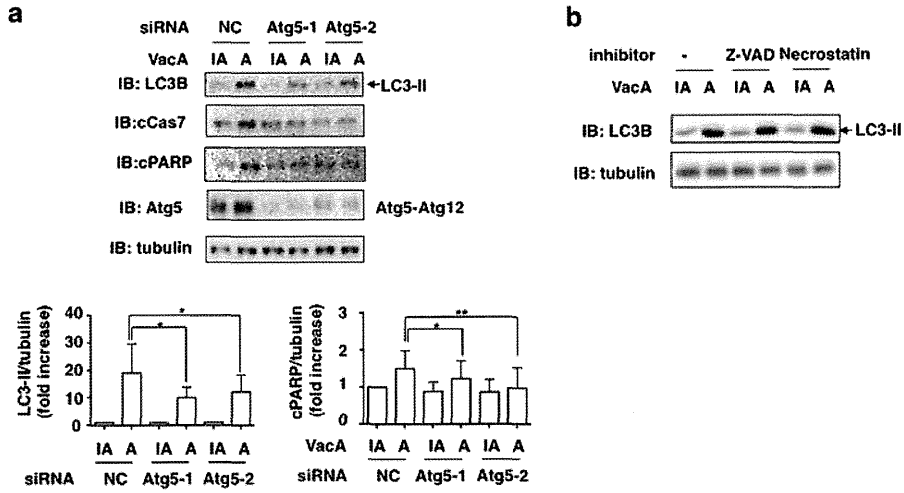

FIGURE 8. **Effects of Atg5 silencing, Z-VAD-fmk, and Necrostatin-1 on VacA-induced LC3-II generation and PARP cleavage.** *a*, the indicated siRNA-transfected AZ-521 cells were incubated with 120 nM heat-inactivated (*IA*) or wild-type VacA (*A*) for 8–10 h at 37 °C and the cell lysates were subjected to immunoblotting (*IB*) with anti-LC3B, anti-cleaved PARP, or anti-Atg5 antibodies. α-Tubulin, as a loading control. A blot representative of three separate experiments is shown. Quantification of VacA-induced LC3-II or PARP cleavage (*cPARP*) in the indicated siRNA-transfected AZ-521 cells was performed by densitometry (*bottom panel*). Data are presented as mean ± S.D. and significance is (*) $p < 0.05$ ($n = 5$) and (**) $p < 0.01$ ($n = 5$). *b*, AZ-521 cells were pretreated with 50 μM Z-VAD-fmk (*Z-VAD*) or 50 μM Necrostatin-1 (*Necrostatin*) for 30 min, and then 120 nM heat-inactivated or wild-type VacA were added to cells. After a 10-h incubation at 37 °C, cell lysates were analyzed by Western blotting using antibodies against LC3B and cleaved PARP. α-Tubulin served as a loading control. Data are representative of three separate experiments. Quantification of VacA-induced PARP cleavage (*cPARP*) levels in the indicated siRNA-transfected AZ-521 cells was performed by densitometry (*bottom panel*). Data are presented as mean ± S.D. and significance is (*) $p < 0.01$ ($n = 3$).

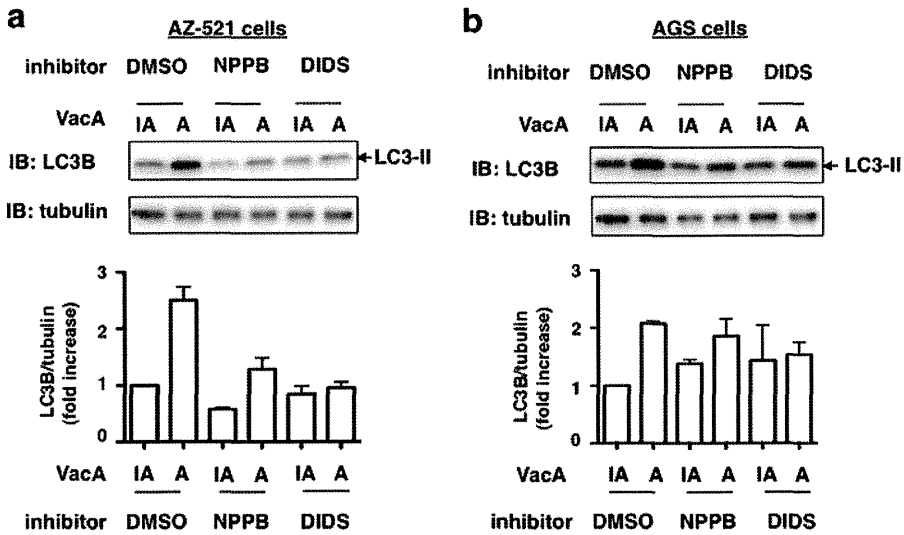

FIGURE 9. **Effect of anion-channel inhibitor on VacA-induced LC3-II generation.** AZ-521 (*a*) or AGS (*b*) cells were pretreated with 100 μM NPPB or DIDS for 30 min at 37 °C and then incubated with 120 nM heat-inactivated (*IA*) or wild-type VacA (*A*) for 4 h at 37 °C. Cell lysates were subjected to immunoblotting (*IB*) with anti-LC3B antibody or anti-α-tubulin antibody as a loading control. Quantification of VacA-induced LC3-II levels in the cells was performed by densitometry (*bottom panel*). Data are mean ± S.D. of values from two independent experiments.

tents. This process is considered cytoprotective but in certain settings excessive autophagy can cause cell death (34, 42). Little information exists concerning the molecular mechanisms underlying the regulation of apoptosis by autophagy. Our data indicate that autophagy induced by VacA does not involve the canonical pathway in which Beclin-1 initiates the generation of autophagosomes by forming a multiprotein complex with class III PI3K, because 3MA, a class III PI3K inhibitor, and silencing of Beclin-1 did not inhibit autophagy induced by VacA (supplemental Fig. S2). The detailed mechanism by which VacA induces autophagy and apoptosis via LRP1 is not clear. Within VacA-intoxicated cells that provoke death signaling via mitochondrial damage, cells attempt to limit damage by seeking what catabolic benefits may be found in autophagy as indicated by Terebiznik *et al.* (29). Therefore, once the stress-provoking, death-signaling response to VacA is overwhelming, autophagy is futile, and it is beneficial to induce apoptosis. Future studies involving mouse models and human specimens will help to determine whether LRP1 plays a critical role in the pathobiology of *H. pylori* infection *in vivo*.

Acknowledgments—We thank K. Maeda for skillful assistance and P. I. Padilla (University of the Philippines Visayas, Philippines) and B. De Guzman (St. Luke's Medical Center, Philippines) for helpful discussions.

REFERENCES

1. Wroblewski, L. E., Peek, R. M., Jr., and Wilson, K. T. (2010) *Helicobacter pylori* and gastric cancer. Factors that modulate disease risk. *Clin. Microbiol. Rev.* **23,** 713–739
2. Yamaoka, Y. (2010) Mechanisms of disease. *Helicobacter pylori* virulence factors. *Nat. Rev. Gastroenterol. Hepatol.* **7,** 629–641
3. Telford, J. L., Ghiara, P., Dell'Orco, M., Comanducci, M., Burroni, D., Bugnoli, M., Tecce, M. F., Censini, S., Covacci, A., and Xiang, Z. (1994) Gene structure of the *Helicobacter pylori* cytotoxin and evidence of its key role in gastric disease. *J. Exp. Med.* **179,** 1653–1658
4. Marchetti, M., Aricò, B., Burroni, D., Figura, N., Rappuoli, R., and Ghiara, P. (1995) Development of a mouse model of *Helicobacter pylori* infection that mimics human disease. *Science* **267,** 1655–1658
5. Ghiara, P., Marchetti, M., Blaser, M. J., Tummuru, M. K., Cover, T. L., Segal, E. D., Tompkins, L. S., and Rappuoli, R. (1995) Role of the *Helicobacter pylori* virulence factors vacuolating cytotoxin, CagA, and urease in a mouse model of disease. *Infect. Immun.* **63,** 4154–4160
6. Kuo, C. H., and Wang, W. C. (2003) Binding and internalization of *Helicobacter pylori* VacA via cellular lipid rafts in epithelial cells. *Biochem. Biophys. Res. Commun.* **303,** 640–644
7. Oldani, A., Cormont, M., Hofman, V., Chiozzi, V., Oregioni, O., Canonici, A., Sciullo, A., Sommi, P., Fabbri, A., Ricci, V., and Boquet, P. (2009) *Helicobacter pylori* counteracts the apoptotic action of its VacA toxin by injecting the CagA protein into gastric epithelial cells. *PLoS Pathog.* **5,** e1000603
8. Akada, J. K., Aoki, H., Torigoe, Y., Kitagawa, T., Kurazono, H., Hoshida, H., Nishikawa, J., Terai, S., Matsuzaki, M., Hirayama, T., Nakazawa, T., Akada, R., and Nakamura, K. (2010) *Helicobacter pylori* CagA inhibits endocytosis of cytotoxin VacA in host cells. *Dis. Model Mech.* **3,** 605–617
9. Kuck, D., Kolmerer, B., Iking-Konert, C., Krammer, P. H., Stremmel, W., and Rudi, J. (2001) Vacuolating cytotoxin of *Helicobacter pylori* induces apoptosis in the human gastric epithelial cell line AGS. *Infect. Immun.* **69,** 5080–5087
10. Cover, T. L., and Blanke, S. R. (2005) *Helicobacter pylori* VacA, a paradigm for toxin multifunctionality. *Nat. Rev. Microbiol.* **3,** 320–332
11. Yamasaki, E., Wada, A., Kumatori, A., Nakagawa, I., Funao, J., Nakayama, M., Hisatsune, J., Kimura, M., Moss, J., and Hirayama, T. (2006) *Helicobacter pylori* vacuolating cytotoxin induces activation of the proapoptotic proteins Bax and Bak, leading to cytochrome *c* release and cell death, independent of vacuolation. *J. Biol. Chem.* **281,** 11250–11259
12. Calore, F., Genisset, C., Casellato, A., Rossato, M., Codolo, G., Esposti, M. D., Scorrano, L., and de Bernard, M. (2010) Endosome-mitochondria juxtaposition during apoptosis induced by *H. pylori* VacA. *Cell Death Differ.* **17,** 1707–1716
13. Jain, P., Luo, Z. Q., and Blanke, S. R. (2011) *Helicobacter pylori* vacuolating cytotoxin A (VacA) engages the mitochondrial fission machinery to induce host cell death. *Proc. Natl. Acad. Sci. U.S.A.* **108,** 16032–16037
14. Papini, E., de Bernard, M., Milia, E., Bugnoli, M., Zerial, M., Rappuoli, R., and Montecucco, C. (1994) Cellular vacuoles induced by *Helicobacter pylori* originate from late endosomal compartments. *Proc. Natl. Acad. Sci. U.S.A.* **91,** 9720–9724
15. Yahiro, K., Niidome, T., Kimura, M., Hatakeyama, T., Aoyagi, H., Kurazono, H., Imagawa, K., Wada, A., Moss, J., and Hirayama, T. (1999) Activation of *Helicobacter pylori* VacA toxin by alkaline or acid conditions increases its binding to a 250-kDa receptor protein-tyrosine phosphatase β. *J. Biol. Chem.* **274,** 36693–36699
16. Yahiro, K., Wada, A., Nakayama, M., Kimura, T., Ogushi, K., Niidome, T., Aoyagi, H., Yoshino, K., Yonezawa, K., Moss, J., and Hirayama, T. (2003) Protein-tyrosine phosphatase α, RPTP α, is a *Helicobacter pylori* VacA receptor. *J. Biol. Chem.* **278,** 19183–19189
17. Hennig, E. E., Godlewski, M. M., Butruk, E., and Ostrowski, J. (2005) *Helicobacter pylori* VacA cytotoxin interacts with fibronectin and alters HeLa cell adhesion and cytoskeletal organization *in vitro*. *FEMS Immunol. Med. Microbiol.* **44,** 143–150
18. Gupta, V. R., Patel, H. K., Kostolansky, S. S., Ballivian, R. A., Eichberg, J., and Blanke, S. R. (2008) Sphingomyelin functions as a novel receptor for *Helicobacter pylori* VacA. *PLoS Pathog.* **4,** e1000073
19. Papadimitriou, E., Mikelis, C., Lampropoulou, E., Koutsioumpa, M., Theochari, K., Tsirmoula, S., Theodoropoulou, C., Lamprou, M., Sfaelou, E., Vourtsis, D., and Boudouris, P. (2009) Roles of pleiotrophin in tumor growth and angiogenesis. *Eur. Cytokine Netw.* **20,** 180–190
20. Fujikawa, A., Shirasaka, D., Yamamoto, S., Ota, H., Yahiro, K., Fukada, M., Shintani, T., Wada, A., Aoyama, N., Hirayama, T., Fukamachi, H., and Noda, M. (2003) Mice deficient in protein-tyrosine phosphatase receptor type Z are resistant to gastric ulcer induction by VacA of *Helicobacter pylori*. *Nat. Genet.* **33,** 375–381
21. Gebert, B., Fischer, W., Weiss, E., Hoffmann, R., and Haas, R. (2003) *Helicobacter pylori* vacuolating cytotoxin inhibits T lymphocyte activation. *Science* **301,** 1099–1102
22. Boncristiano, M., Paccani, S. R., Barone, S., Ulivieri, C., Patrussi, L., Ilver, D., Amedei, A., D'Elios, M. M., Telford, J. L., and Baldari, C. T. (2003) The *Helicobacter pylori* vacuolating toxin inhibits T cell activation by two independent mechanisms. *J. Exp. Med.* **198,** 1887–1897
23. Sewald, X., Gebert-Vogl, B., Prassl, S., Barwig, I., Weiss, E., Fabbri, M., Osicka, R., Schiemann, M., Busch, D. H., Semmrich, M., Holzmann, B., Sebo, P., and Haas, R. (2008) Integrin subunit CD18 Is the T-lymphocyte receptor for the *Helicobacter pylori* vacuolating cytotoxin. *Cell Host Microbe* **3,** 20–29
24. Sewald, X., Jimenez-Soto, L., and Haas, R. (2011) PKC-dependent endocytosis of the *Helicobacter pylori* vacuolating cytotoxin in primary T lymphocytes. *Cell Microbiol.* **13,** 482–496
25. Cover, T. L., Krishna, U. S., Israel, D. A., and Peek, R. M., Jr. (2003) Induction of gastric epithelial cell apoptosis by *Helicobacter pylori* vacuolating cytotoxin. *Cancer Res.* **63,** 951–957
26. Singh, M., Prasad, K. N., Saxena, A., and Yachha, S. K. (2006) *Helicobacter pylori* induces apoptosis of T- and B-cell lines and translocates mitochondrial apoptosis-inducing factor to nucleus. *Curr. Microbiol.* **52,** 254–260
27. Radin, J. N., Gonzalez-Rivera, C., Ivie, S. E., McClain, M. S., and Cover, T. L. (2011) *Helicobacter pylori* VacA induces programmed necrosis in gastric epithelial cells. *Infect. Immun.* **79,** 2535–2543
28. Raju, D., Hussey, S., Ang, M., Terebiznik, M. R., Sibony, M., Galindo-Mata, E., Gupta, V., Blanke, S. R., Delgado, A., Romero-Gallo, J., Ramjeet, M. S., Mascarenhas, H., Peek, R. M., Correa, P., Streutker, C., Hold, G., Kunstmann, E., Yoshimori, T., Silverberg, M. S., Girardin, S. E., Philpott, D. J., El Omar, E., and Jones, N. L. (2012) Vacuolating cytotoxin and variants in Atg16L1 that disrupt autophagy promote *Helicobacter pylori* infection in humans. *Gastroenterology* **142,** 1160–1171
29. Terebiznik, M. R., Raju, D., Vázquez, C. L., Torbricki, K., Kulkarni, R., Blanke, S. R., Yoshimori, T., Colombo, M. I., and Jones, N. L. (2009) Effect of *Helicobacter pylori*'s vacuolating cytotoxin on the autophagy pathway in gastric epithelial cells. *Autophagy* **5,** 370–379
30. Lum, J. J., Bauer, D. E., Kong, M., Harris, M. H., Li, C., Lindsten, T., and Thompson, C. B. (2005) Growth factor regulation of autophagy and cell survival in the absence of apoptosis. *Cell* **120,** 237–248
31. Gozuacik, D., and Kimchi, A. (2004) Autophagy as a cell death and tumor suppressor mechanism. *Oncogene* **23,** 2891–2906
32. McPhee, C. K., Logan, M. A., Freeman, M. R., and Baehrecke, E. H. (2010) Activation of autophagy during cell death requires the engulfment receptor Draper. *Nature* **465,** 1093–1096
33. Wirawan, E., Vande Walle, L., Kersse, K., Cornelis, S., Claerhout, S., Vanoverberghe, I., Roelandt, R., De Rycke, R., Verspurten, J., Declercq, W., Agostinis, P., Vanden Berghe, T., Lippens, S., and Vandenabeele, P. (2010) Caspase-mediated cleavage of Beclin-1 inactivates Beclin-1-induced autophagy and enhances apoptosis by promoting the release of proapoptotic factors from mitochondria. *Cell Death Dis.* **1,** e18
34. Maiuri, M. C., Criollo, A., and Kroemer, G. (2010) Cross-talk between apoptosis and autophagy within the Beclin 1 interactome. *EMBO J.* **29,** 515–516
35. Rubinstein, A. D., Eisenstein, M., Ber, Y., Bialik, S., and Kimchi, A. (2011) The autophagy protein Atg12 associates with antiapoptotic Bcl-2 family members to promote mitochondrial apoptosis. *Mol. Cell* **44,** 698–709
36. Nakayama, M., Hisatsune, J., Yamasaki, E., Nishi, Y., Wada, A., Kurazono, H., Sap, J., Yahiro, K., Moss, J., and Hirayama, T. (2006) Clustering of *Helicobacter pylori* VacA in lipid rafts, mediated by its receptor, receptor-like protein-tyrosine phosphatase β, is required for intoxication in AZ-521

cells. *Infect. Immun.* **74,** 6571–6580
37. Høyer-Hansen, M., Bastholm, L., Mathiasen, I. S., Elling, F., and Jäättelä, M. (2005) Vitamin D analog EB1089 triggers dramatic lysosomal changes and Beclin 1-mediated autophagic cell death. *Cell Death Differ.* **12,** 1297–1309
38. Yang, S., Wang, X., Contino, G., Liesa, M., Sahin, E., Ying, H., Bause, A., Li, Y., Stommel, J. M., Dell'antonio, G., Mautner, J., Tonon, G., Haigis, M., Shirihai, O. S., Doglioni, C., Bardeesy, N., and Kimmelman, A. C. (2011) Pancreatic cancers require autophagy for tumor growth. *Genes Dev.* **25,** 717–729
39. Youle, R. J., and Narendra, D. P. (2011) Mechanisms of mitophagy. *Nat. Rev. Mol. Cell Biol.* **12,** 9–14
40. Vives-Bauza, C., and Przedborski, S. (2011) Mitophagy. The latest problem for Parkinson disease. *Trends Mol. Med.* **17,** 158–165
41. Kirkin, V., McEwan, D. G., Novak, I., and Dikic, I. (2009) A role for ubiquitin in selective autophagy. *Mol. Cell* **34,** 259–269
42. Yoshimori, T. (2007) Autophagy. Paying Charon's toll. *Cell* **128,** 833–836
43. Zhu, H., Fearnhead, H. O., and Cohen, G. M. (1995) An ICE-like protease is a common mediator of apoptosis induced by diverse stimuli in human monocytic THP.1 cells. *FEBS Lett.* **374,** 303–308
44. Degterev, A., Huang, Z., Boyce, M., Li, Y., Jagtap, P., Mizushima, N., Cuny, G. D., Mitchison, T. J., Moskowitz, M. A., and Yuan, J. (2005) Chemical inhibitor of nonapoptotic cell death with therapeutic potential for ischemic brain injury. *Nat. Chem. Biol.* **1,** 112–119
45. Tombola, F., Carlesso, C., Szabò, I., de Bernard, M., Reyrat, J. M., Telford, J. L., Rappuoli, R., Montecucco, C., Papini, E., and Zoratti, M. (1999) *Helicobacter pylori* vacuolating toxin forms anion-selective channels in planar lipid bilayers. Possible implications for the mechanism of cellular vacuolation. *Biophys. J.* **76,** 1401–1409
46. Montecucco, C., and Rappuoli, R. (2001) Living dangerously. How *Helicobacter pylori* survives in the human stomach. *Nat. Rev. Mol. Cell Biol.* **2,** 457–466
47. Boquet, P., and Ricci, V. (2012) Intoxication strategy of *Helicobacter pylori* VacA toxin. *Trends Microbiol.* **20,** 165–174
48. Szabò, I., Brutsche, S., Tombola, F., Moschioni, M., Satin, B., Telford, J. L., Rappuoli, R., Montecucco, C., Papini, E., and Zoratti, M. (1999) Formation of anion-selective channels in the cell plasma membrane by the toxin VacA of *Helicobacter pylori* is required for its biological activity. *EMBO J.* **18,** 5517–5527
49. Foo, J. H., Culvenor, J. G., Ferrero, R. L., Kwok, T., Lithgow, T., and Gabriel, K. (2010) Both the p33 and p55 subunits of the *Helicobacter pylori* VacA toxin are targeted to mammalian mitochondria. *J. Mol. Biol.* **401,** 792–798
50. Torres, V. J., Ivie, S. E., McClain, M. S., and Cover, T. L. (2005) Functional properties of the p33 and p55 domains of the *Helicobacter pylori* vacuolating cytotoxin. *J. Biol. Chem.* **280,** 21107–21114
51. Isomoto, H., Moss, J., and Hirayama, T. (2010) Pleiotropic actions of *Helicobacter pylori* vacuolating cytotoxin, VacA. *Tohoku J. Exp. Med.* **220,** 3–14
52. Herz, J., and Strickland, D. K. (2001) LRP. A multifunctional scavenger and signaling receptor. *J. Clin. Invest.* **108,** 779–784
53. Salicioni, A. M., Gaultier, A., Brownlee, C., Cheezum, M. K., and Gonias, S. L. (2004) Low density lipoprotein receptor-related protein-1 promotes beta1 integrin maturation and transport to the cell surface. *J. Biol. Chem.* **279,** 10005–10012
54. Genisset, C., Puhar, A., Calore, F., de Bernard, M., Dell'Antone, P., and Montecucco, C. (2007) The concerted action of the *Helicobacter pylori* cytotoxin VacA and of the v-ATPase proton pump induces swelling of isolated endosomes. *Cell Microbiol.* **9,** 1481–1490

Dig Dis Sci (2013) 58:354–362
DOI 10.1007/s10620-012-2350-x

ORIGINAL ARTICLE

Attenuation of Acetic Acid-Induced Gastric Ulcer Formation in Rats by Glucosylceramide Synthase Inhibitors

Manabu Nakashita · Hidekazu Suzuki · Soichiro Miura · Takao Taki · Keita Uehara · Tohru Mizushima · Hiroshi Nagata · Toshifumi Hibi

Received: 10 May 2012 / Accepted: 28 July 2012 / Published online: 24 August 2012

Abstract
Introduction Ceramide has been suggested to play a role in apoptosis during gastric ulcerogenesis. The present study is designed to investigate whether accumulated ceramide could serve as the effector molecules of ulcer formation in a rat model of acetic acid-induced gastric ulcer.
Methods The effect of fumonisin B1, an inhibitor of ceramide synthase, and of *d,l,-threo*-1-phenyl-2-hexadecanoylamino-3-morpholino-1-propanol (PPMP) and N-butyldeoxynojirimycin (NB-DNJ), both inhibitors of glucosylceramide synthase, on the accumulation of ceramide and formation of gastric ulcer were examined in the rat model of acetic acid-induced gastric ulcer.
Results Fumonisin B1 attenuated acetic acid-induced gastric ulcer formation, associated with a decrease in the number of apoptotic cells. Our results showed that it is neither the C18- nor the C24-ceramide itself, but the respective metabolites that were ulcerogenic, because PPMP and NB-DNJ attenuated gastric mucosal apoptosis and the consequent mucosal damage in spite of their reducing the degradation of ceramide.
Conclusion The ceramide pathway, in particular, the metabolites of ceramide, significantly contributes to acetic acid-induced gastric damage, possibly via enhancing apoptosis. On the other hand, PPMP and NB-DNJ treatment attenuated gastric mucosal apoptosis and ulcer formation despite increasing the ceramide accumulation, suggesting that it was not the ceramides themselves, but their metabolites that contributed to the ulcer formation in the acetic acid-induced gastric ulcer model.

Keywords Ceramide · Glucosylceramide inhibitor · Gastric ulcer · Acetic acid · Apoptosis

M. Nakashita · H. Suzuki (✉) · K. Uehara · H. Nagata · T. Hibi
Division of Gastroentrology and Hepatology, Department of Internal Medicine, School of Medicine, Keio University, 35 Shinanomachi, Shinjuku-ku, Tokyo 160-8582, Japan
e-mail: hsuzuki@a6.keio.jp

M. Nakashita · H. Nagata
Department of Internal Medicine, Keiyu Hospital, Yokohama, Japan

S. Miura
Second Department of Internal Medicine, National Defense Medical College, Saitama, Japan

T. Taki
Molecular Medical Science Institute, Otsuka Pharmaceutical Co. Ltd, Tokushima, Japan

T. Mizushima
Faculty of Pharmacy, Keio University, Tokyo, Japan

Introduction

While many factors have been thought to be involved in the pathogenesis of gastric ulcers, the mechanism of ulcer formation is not yet precisely understood. Gastric mucosal apoptosis is known to be associated with the loss of mucosal integrity and may play an important role in ulcer development [1, 2]. Recently, enhanced apoptosis in the gastric epithelium has been demonstrated to be of pathophysiological importance in various kinds of gastric lesions, such as stress-induced ulcers [1], *Helicobacter pylori*-positive ulcers [3–5], nonsteroidal anti-inflammatory drug (NSAID)-induced ulcers [6], and chemically induced ulcers, such as ethanol-induced ulcers [7, 8]. Inflammatory cytokines, including tumor necrosis factor (TNF)-α and interferon (IFN)-γ, have been postulated to play a role in gastric mucosal apoptosis [8].

Recent studies have revealed that sphingolipids (ceramide, sphingosine, etc.) are highly bioactive compounds that are involved in diverse cell processes, including cell-to-cell interactions, adhesion, differentiation and oncogenic transformation [9], as well as cell proliferation and apoptosis. Accumulation of the sphingolipid ceramide (Cer) is a well-known phenomenon in cells undergoing apoptosis [10, 11], and ceramide analogues have been reported to induce apoptosis [12]. In addition to their direct action on apoptosis, ceramides have also been suggested to have a role in apoptosis induced by the addition of extracellular agents, such as TNF-α [13, 14], IFN-γ [15] or the anti-Fas antibody [16].

Ceramide analogues have been demonstrated in vitro to induce apoptosis in gastric mucosal cell lines. We previously reported that the subserosal injection of phorbol-12-myristate-13-acetate (PMA) resulted in the formation of gastric ulcers in the rat gastric mucosa [17], associated with a significant increase in the cellular contents of ceramides (C18 and C24 ceramide) [18]. The significant ceramide accumulation was thought to have contributed to the PMA-induced tissue damage in that rat model, possibly via enhancing the apoptotic activity in the gastric mucosa, because co-administration of caspase inhibitors or an inhibitor of sphingolipid biosynthesis attenuated the formation of the gastric ulcers, associated with a reduction in the number of apoptotic cells [18]. However, it remains unknown whether the ceramide-induced gastric mucosal damage was evoked specifically only by the PMA injection or whether the ceramide pathway is also, in general, involved in the formation of gastric ulcers induced by various factors. It is also important to elucidate what kind of downstream molecules may be involved in gastric ulcer formation after ceramide activation.

Ceramide is produced from sphingosine (sphinganine) by sphingosine N-acyltransferase (ceramide synthase), which is potentially inhibited by fumonisin B1. Glucosylceramide synthase (GCS) is a ceramide glucosyl transferase that processes the sphingolipid ceramide [19]. This conversion of ceramide to glucosylceramide is prevented by *d,l,-threo*-1-phenyl-2-hexadecanoylamino-3-morpho-lino-1-propanol (PPMP) and N-butyldeoxynojirimycin (NB-DNJ) [20, 21]. The product, glucosylceramide, can be further elaborated with a variety of oligosaccharides to become glycosphingolipids called gangliosides such as GM3 (monosialoganglioside 3) and GD3 (disialoganglioside 3) [19] (Fig. 1).

To answer these questions, we investigated the ceramide formation and induction of apoptosis and gastric mucosal damage during the gastric ulcer formation process using a rat model of acetic acid-induced gastric ulcer, which is a representative experimental model of chronic gastric ulcer. We also examined the effects of two different kinds of glucosylceramide synthase inhibitors on the gastric ulcer formation induced by acetic acid, to investigate whether it was the ceramides themselves or their metabolites that were involved in the pathogenesis of the gastric ulcers.

Materials and Methods

Animals and Ulcer Induction

Male Sprague-Dawlay rats, weighing 200–250 g and maintained on standard laboratory chow (Oriental Yeast Mfg., Ltd., Tokyo, Japan) were used for all the experiments. All the animals were handled according to the guidelines of the Animal Research Committee of Keio University School of Medicine. The rats were denied any food for 24 h prior to the experiments, but were allowed access to tap water ad libitum. Gastric ulcers were induced by injection of an acetic acid solution [22]. Vehicle (water) was injected as a control. In brief, the abdomen of the animals, under anesthesia with 30 mg/kg of pentobarbital sodium, was opened via a midline incision. The stomach was exposed and 50 μl of either 20 % acetic acid or vehicle (water) was injected into the subserosa of the anterior wall of the glandular stomach using a microsyringe, followed by closure of the abdomen.

At different time intervals (24, 48, and 72 h) after the injection of acetic acid or vehicle, the rats were sacrificed with an overdose of sodium pentobarbital. Their stomachs were quickly removed, opened along the greater curvature, and rinsed with cold normal saline. The surface area of each lesion in the gastric mucosa was assessed visually by macroscopic examination. The ulcer area was calculated as an area of similarity ellipse (ulcer area = $\pi^*a^*b^*1/4$; a major axis, b minor axis).

Administration of Various Inhibitors

To examine the changes in the gastric mucosal ceramide contents in this model, an inhibitor of sphingolipid biosynthesis, fumonisin B1 (FB1), was injected concomitantly (0.036–0.09 g/kg body weight) (Sigma) [23] with the acetic acid into the gastric subserosa. To determine the role of glucosylceramide in the acetic acid-induced ulcer formation, we used two types of inhibitors of glucosylceramide synthase, namely, *d,l,-threo*-1-phenyl-2-hexadecanoylamino-3-morpholino-1-propanol (PPMP) (0.0127–1.27 g/kg body weight) (Sigma-Aldrich) and N-butyldeoxynojirimycin (NB-DNJ) (0.11–11 g/kg body weight) (Sigma-Aldrich), which prevent the conversion of ceramide to glucosylceramide [20, 21]. These inhibitors were also injected concomitantly with acetic acid into the gastric subserosa. To prevent any systemic effects of the ceramide inhibitors as well as any

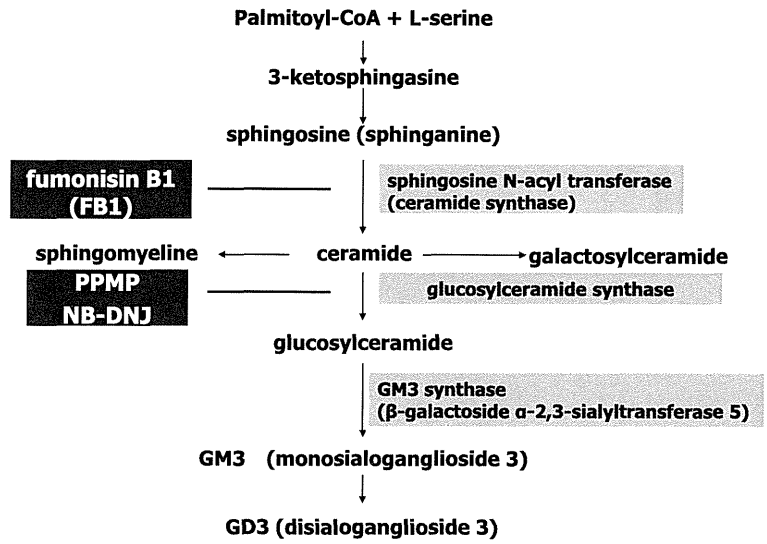

Fig. 1 Pathway of ceramide metabolism

possible interaction with acetic acid, ceramide inhibitors were injected locally with acetic acid by mixing just before the injection.

Determination of the Ceramide Contents in the Stomach

The time-course of changes of the ceramide contents in the stomach was examined. The excised stomachs were cut along the greater curvature and rinsed with physiological saline. Approximately 0.5 g of the tissue sample including the ulcer lesions was removed and minced, and lipid extraction was performed using a modified version of the method described by Bligh and Dyer [24]. After extracting the major lipids, the neutral lipids, including the ceramides, were separated by high-performance thin-layer chromatography (HPTLC) (Silicagel 60, Merck, Germany). The dried lipids were then resolved by thin-layer chromatography using petroleum ether/diethyl ether (7:3) as the first solvent, and chloroform/methanol (95:5) as the second solvent. After separating the lipids, the HPTLC plate was sprayed with a primulin reagent until it was thoroughly wet and then air-dried completely. The lipids were visualized under UV light at 365 nm and analyzed with a densitometer (Fluorchem^{TM} 8000, Alpha Innotech Co., San Leandro, CA, USA). Furthermore, the glucosylceramide and GM3 contents in the stomach were also examined according to the above-mentioned procedure. After the glycosphingolipids were separated by TLC, chloroform/methanol/0.2 % aqueous $CaCl_2$(60/35/8, by volume) was used as the developing agent for the TLC plates. GM3 was visualized by spraying the plate with orcinol-H_2SO_4 reagent. The lipids were visualized under UV light at 365 nm.

Determination of the Degree of Apoptosis in the Gastric Mucosa

Apoptosis was determined by immunohistochemical staining with a polyclonal antibody to ss-DNA. The area of the stomach containing the ulcer was rapidly excised and processed using routine techniques, followed by embedding in paraffin. Sections (4-μm thick) were then prepared and mounted on glass slides. Deparaffinized sections were treated with 3 % hydrogen peroxide for 20 min to block endogenous peroxide. Then, after blocking with 10 % non-immune serum for 10 min at room temperature, the sections were incubated for 40 min at room temperature with a primary antibody (anti-ss-DNA, polyclonal rabbit, DAKO, Carpinteria, CA, USA) diluted 1:100 with 0.1 % bovine serum albumin (BSA) in 0.05 M tris-buffered saline (TBS). The slides were washed three times with 0.05 M TBS-Tween for 5 min, followed by incubation for 30 min with rabbit peroxidase (DAKO). After washing for 5 min in TBS-Tween, the sections were stained using a diaminobenzidine reagent kit (Kirkegaard & Perry Laboratory Inc., Gaithersburg, USA) and observed under a microscope (Nikon ECLIPSE-E-600, Tokyo, Japan). Negative controls containing non-immune rabbit serum with omission of the primary antibody were also prepared. Staining for all antibodies was assessed in a blinded manner by the same observer.

Statistical Analysis

All results were expressed as the mean ± SEM. Differences among groups were evaluated using one-way analysis of variance (ANOVA) and Fisher's post hoc test. Statistical significance was set at $p < 0.05$.

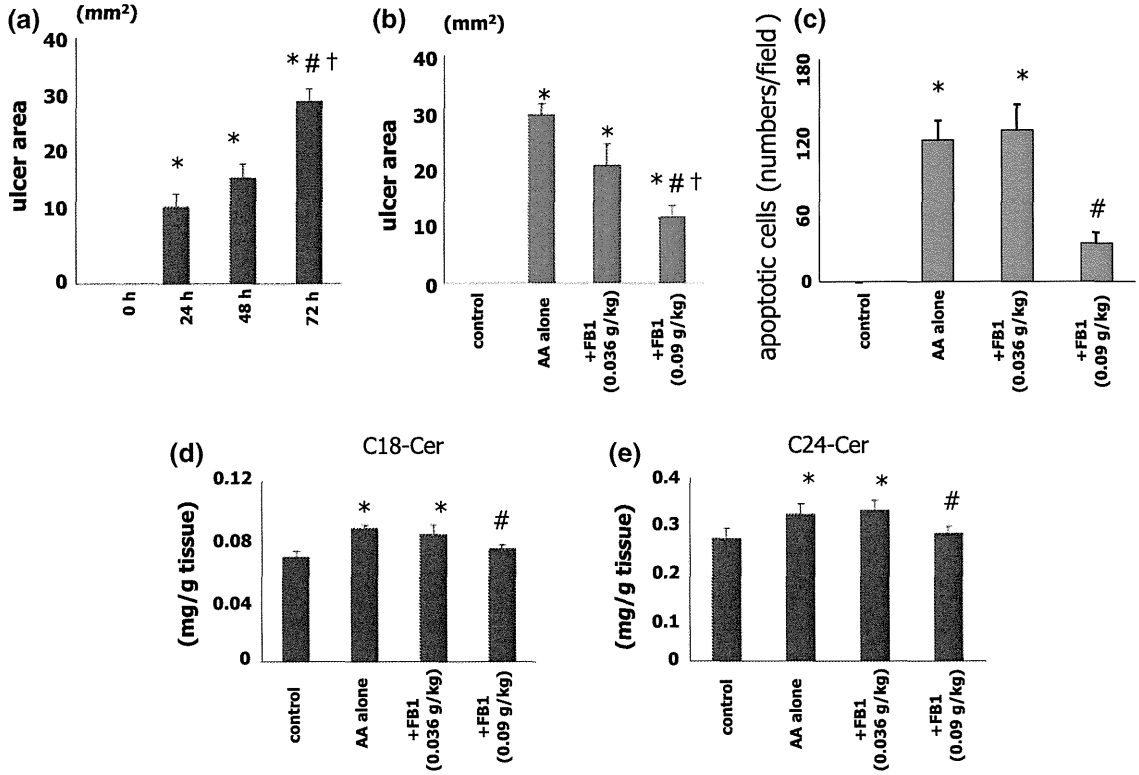

Fig. 2 **a** Time-course of changes in the area of the mucosal lesions after subserosal injection of 20 % acetic acid (50 µl). * $p < 0.05$ vs. 0 h, # $p < 0.05$ vs. 24 h, † $p < 0.05$ vs. 48 h. Each *bar* indicates mean value with SEM of six animals. **b** Inhibitory effects of different concentrations of fumonisin B1 (FB1; 0.036–0.09 g/kg body weight) on acetic acid-induced gastric ulcer formation at 72 h after the injection. Vehicle (water) was injected as a control. The ulcer index is expressed as the area of the mucosal lesions (mm^2). * $p < 0.05$ vs. control. # $p < 0.05$ vs. acetic acid alone. † $p < 0.01$ vs. FB1 (0.036 g/kg body weight). Values are mean ± SEM in six animals. **c** Effects of FB1 on the number of apoptotic cells appearing in the gastric mucosa at 72 h after acetic acid administration. The apoptotic cell number was determined in sections stained immunohistochemically with a polyclonal antibody against ss-DNA, and expressed as the average number of positively stained cells per microscopic field (×400). FB1 at 25 µM significantly attenuated the increase in the number of apoptotic cells induced by acetic acid administration. * $p < 0.05$ vs. control (vehicle); # $p < 0.05$ vs. acetic acid alone. Values are mean ± SEM in six animals. **d, e** Ceramide contents in the gastric mucosa at 72 h after acetic acid subserosal injection, and the inhibitory effect of FB1. Four samples were loaded on HPLC plates and densitometric analysis of the C18- (d) and C24- (e) ceramide contents was performed as described in "Materials and Methods". * $p < 0.05$ vs. control. # $p < 0.05$ vs. acetic acid alone. Values are mean ± SEM in six animals

Results

Effect of Fumonisin B1 on Acetic Acid-Induced Ulcer Formation

Figure 2a shows the time-course of changes in the area of the mucosal lesions, and Fig. 2b shows the inhibitory effects of different concentrations of fumonisin B1 (FB1; 0.036 and 0.09 g/kg body weight) on the area of the lesions after 72 h. The ulcers produced by the acetic acid injection began to form at the injection site in the stomach, expanded to their maximum size after 72 h, and healed gradually from day 5 to day 8 (data not shown). The ulcer formation was significantly inhibited by FB1 at the dose of 0.09 g/kg.

Figure 2c shows the number of apoptotic cells in the gastric mucosa at 72 h after the acetic acid injection as assessed immunohistochemically by light microscopy. A significant increase in the number of apoptotic cells was observed at 72 h after the acetic acid injection. FB1 at 0.036 g/kg did not significantly inhibit the acetic acid-induced apoptosis at 72 h, but the drug at 0.09 g/kg significantly attenuated the increase in the frequency of apoptosis induced by acetic acid at 72 h, which is consistent with the inhibition of ulcer formation by the drug. Figure 2d, e shows the C18- (2d) and C24- (2e) ceramide contents in the gastric mucosal lesions at 72 h after the acetic acid injection, and the inhibitory effect of FB1 on the accumulation of ceramides. The amounts of both the C18 and C24 ceramide were significantly increased at 72 h after the acetic acid injection, but not at 24 or 48 h after the injection (data not shown). The increase in the contents of the C18 and C24 ceramides in response to acetic acid injection was significantly attenuated by co-injection of FB1 (0.09 g/kg).

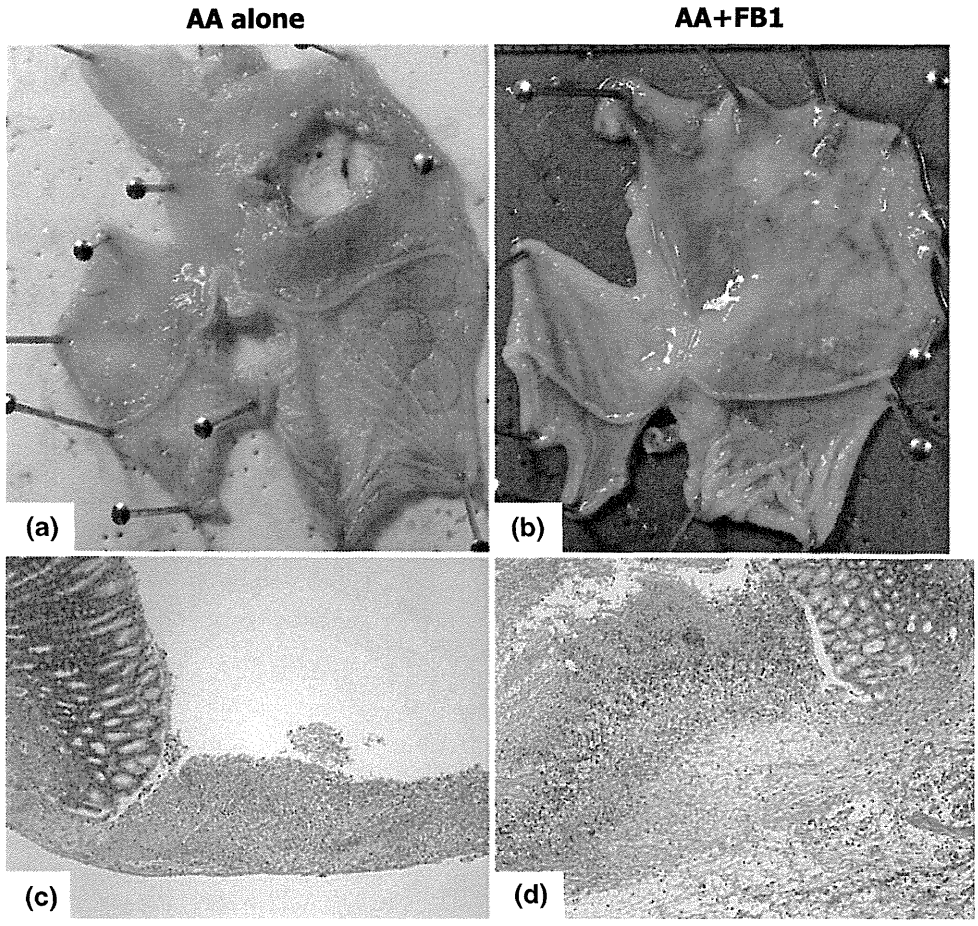

Fig. 3 Representative macroscopic findings were shown. **a** Acetic acid-induced gastric ulcer 72 h after subserosal injection. **b** Acetic acid-induced ulcer formation 72 h after subserosal injection was attenuated by the application of fumonisin B1 (0.09 g/kg body weight). **c**, **d** Representative hematoxylin-eosin (H&E)-stained histopathological findings were shown. **c** Acetic acid-induced ulcer 72 h after subserosal injection (×10). **d** Acetic acid-induced ulcer 72 h after subserosal injection was attenuated by fumonisin B1 (0.09 g/kg body weight) application (×10)

Figure 3a shows the representative macroscopic findings of acetic acid (AA)-induced gastric ulcer. As shown in Fig. 3b, AA-induced ulcer formation was attenuated by the application of FB1. Figure 3c shows the representative histopathological (hematoxylin-eosin staining) finding of AA-induced ulcer. As in Fig. 3d, such AA-induced-ulcer was attenuated by FB1 application.

Effect of PPMP on Acetic Acid-Induced Ulcer Formation

Figure 4a shows the effect of the glucosylceramide synthase inhibitor, PPMP, on acetic acid-induced gastric ulcer formation. PPMP at concentrations of over 0.127 g/kg body weight attenuated the sizes of the acetic acid-induced gastric mucosal lesions at 72 h after treatment.

Figure 4b shows the effect of PPMP on the number of apoptotic cells in the gastric mucosa at 72 h after acetic acid injection. Co-injection of PPMP with acetic acid at doses of over 0.127 g/kg significantly inhibited the acetic acid-induced increase in the number of apoptotic cells which is consistent with the inhibition of ulcer formation by the drug. Figure 4c, d shows a quantitative analysis of the contents of the C18- (4c) and C24- (4d) ceramide after acetic acid injection and the effect of PPMP. The increase in the amounts of both the C18- and C24-ceramide observed at 72 h after acetic acid injection was further enhanced by the concomitant injection of PPMP, and significantly greater amounts of the ceramides were found in the lesions following injection of PPMP at doses higher than 0.127 g/kg.

Effect of NB-DNJ on Acetic Acid-Induced Ulcer Formation

Figure 5a shows the effect of another glucosylceramide synthase inhibitor, NB-DNJ, on acetic acid-induced gastric ulcer formation. Co-injection of NB-DNJ with acetic acid at doses of over 1.1 g/kg body weight significantly attenuated the formation of the gastric mucosal lesions observed at 72 h after the acetic acid injection. Figure 5b shows the effect of NB-DNJ on the number of apoptotic cells appearing in the gastric mucosa at 72 h after the acetic acid injection. Co-injection of NB-DNJ at doses of over 0.11 g/kg body weight significantly attenuated the acetic acid-induced apoptosis in the gastric mucosa. Figure 5c, d shows the effect of NB-DNJ on the contents of the C18- (5c) and C24- (5d) ceramide at 72 h after acetic acid injection. The C18- and C24-ceramide contents significantly increased following

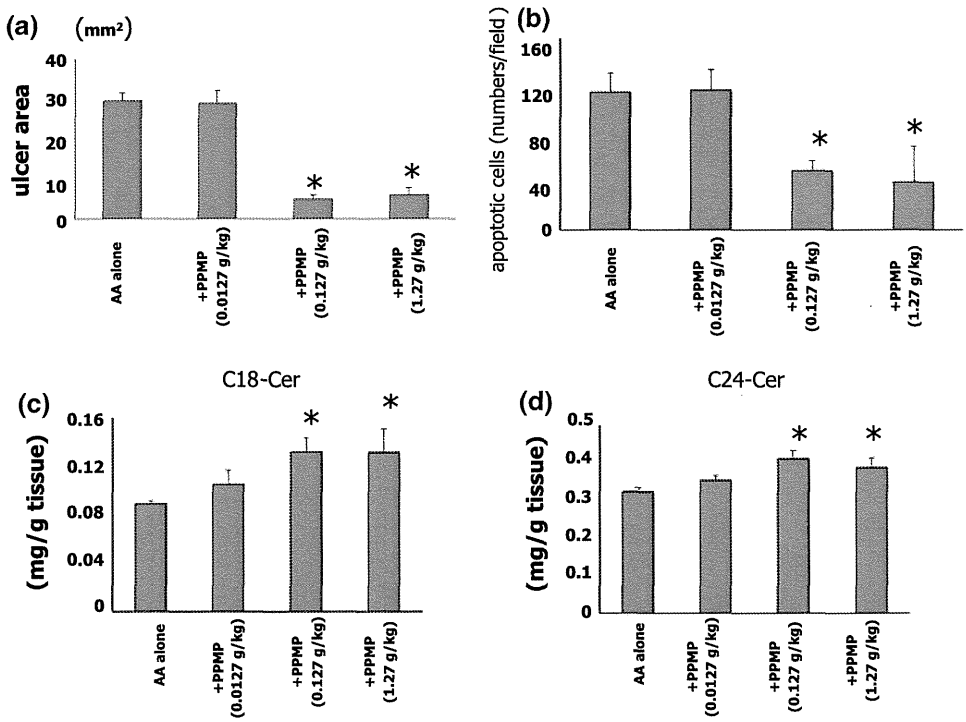

Fig. 4 Each *bar* indicates mean value with SEM of six animals. **a** Effect of the glucosylceramide synthase inhibitor, PPMP, on acetic acid-induced gastric ulcer formation at 72 h after treatment. PPMP (0.0127–1.27 g/kg body weight) was injected concomitantly with acetic acid into the gastric subserosa. * $p < 0.05$ vs. acetic acid alone. Values are mean ± SEM in six animals. **b** Effect of PPMP on the number of apoptotic cells appearing in the gastric mucosa at 72 h after acetic acid administration. PPMP (0.0127–1.27 g/kg body weight) was injected concomitantly with acetic acid into the gastric subserosa. * $p < 0.05$ vs. acetic acid alone. **c**, **d** C18- (c) and C24- (d) ceramide contents observed in the gastric mucosa at 72 h after acetic acid administration. PPMP (0.0127–1.27 g/kg body weight) was injected concomitantly with acetic acid into the gastric subserosa. * $p < 0.05$ vs. acetic acid alone. Values are mean ± SEM in six animals

co-injection of NB-DNJ (1.1 g/kg body weight) as compared with that observed following the injection of acetic acid alone, reflecting the decreased conversion of ceramide to glycosylceramide in these situations.

Glucosylceramide and GM3 on Acetic Acid-Induced Ulcer Formation

Figure 6 shows glucosylceramide and GM3 expressions in acetic acid-induced ulcer formation. The glucosylceramide levels were remarkably low in the acetic acid-induced ulcer group than in the control group. The level of ganglioside GM3 was observed to be high in the acetic acid-induced ulcer group. The expression of GM3 was suppressed and that of glucosylceramide were not restored by the treatment with glucosylceramide synthase inhibitors (PPMP, NB-DNJ).

Discussion

Our present results showing that the blockade of ceramide synthase by fumonisin B1 attenuates acetic acid-induced gastric ulcer formation suggest the importance of de novo ceramide synthesis in the process of ulcer formation induced by acetic acid. Although ceramides, which are derived from the hydrolysis of sphingomyelin in response to extracellular signals, appear to be important in most pathways [10], ceramide synthase-mediated processes, such as the acylation of sphinganine in the de novo biosynthetic pathway of sphingolipids as well as the reutilization of sphingosine derived from sphingolipid turnover [23, 25] may mainly account for the bioactive roles of ceramides in ulcer formation. In this study, we demonstrated an increase in the number of apoptotic cells in the gastric mucosa at 3 h after the injection of acetic acid, with subsequent extension of the lesion area containing apoptotic cells toward the submucosa, as well as a significant attenuation of the increase in acetic acid-induced apoptosis by co-injection of fumonisin B1. These findings suggest that the ceramide pathway may account for the acetic acid-induced ulcer formation via enhancing apoptotic cell death in the damaged mucosa. Our results also confirmed the significant role of the ceramide pathway in other specific experimental models of ulcers, such as PMA-induced gastric ulcers, besides that in the prototype model, namely, the model of acetic acid-induced ulcer [22].

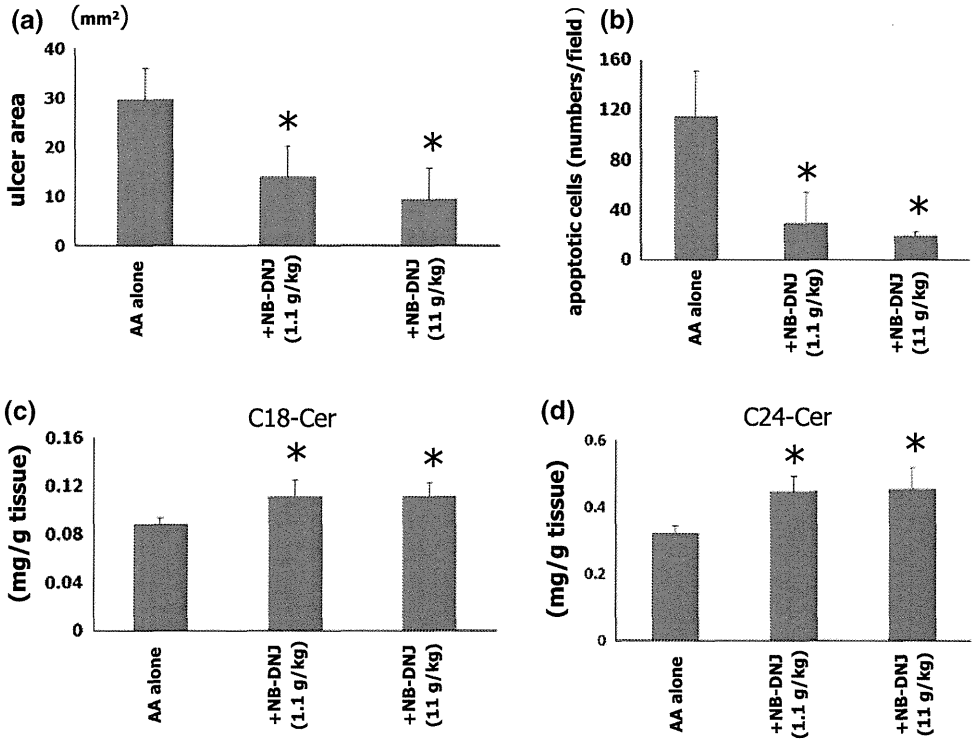

Fig. 5 Each *bar* indicates mean value with SEM of six animals. **a** Effect of NB-DNJ on acetic acid-induced gastric ulcer formation at 72 h after NB-DNJ (0.11–11 g/kg body weight) concomitant administration of the NB-DNJ with acetic acid into the gastric subserosa. * $p < 0.05$ vs. acetic acid alone. Values are the mean ± SEM in six animals. **b** Effect of NB-DNJ on the number of apoptotic cells appearing in the gastric mucosa at 72 h after acetic acid administration. NB-DNJ (0.11–11 g/kg body weight) was injected concomitantly with acetic acid into the gastric subserosa. * $p < 0.05$ vs. acetic acid alone. **c, d** Effect of NB-DNJ on the C18- (c) and C24- (d) ceramide contents observed in the gastric mucosa at 72 h after acetic acid administration. NB-DNJ (0.11–11 g/kg body weight) was injected concomitantly with acetic acid into the gastric subserosa. * $p < 0.05$ vs. acetic acid alone. Values are mean ± SEM in six animals

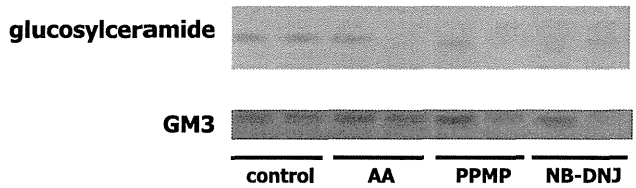

Fig. 6 Effect of PPMP (1.27 g/kg body weight) and NB-DNJ (11 g/kg body weight) on the glucosylceramide and GM3 after subserosal injection of 20 % acetic acid (50 μl). Representative pictures of thin layer chromatography of the glucosylceramide (*upper*) and GM3 (*lower*). Control: H_2O (sterile water) injection

In the present study, we demonstrated that the product of glucosylceramide synthase and not a ceramide itself induces apoptosis, and thus, glucosylceramide synthase inhibitors will decrease apoptosis. The reason for this decrease might be that apoptosis is induced by the product of glucosylceramide synthase.

In our previous manuscript [18], we only examined the increase in the ceramide (C18, C24) levels; we did not evaluate the levels of the ceramide metabolites. However, we showed that the increase in apoptosis in the gastric mucosa corresponded with the increase in the levels of C18 and C24 ceramide in the stomach wall, and that apoptosis was involved in the formation of gastric ulcers induced by PMA (phorbol 12-myristate 13-acetate). Although we previously suggested that ceramide or ceramide metabolites could be ulcerogenic [18], which of the two is ulcerogenic was not determined. In this context, in the previous study, a possibility that ceramide or ceramide metabolites could be a cause of ulcers was established. Our present results indicated that it is neither the C18- nor the C24-ceramide itself, but the respective metabolites that may be ulcerogenic, because we found, to our surprise, that glucosylceramide synthase inhibitors that reduce the degradation of ceramide can also attenuate the gastric mucosal damage induced by acetic acid. We used two types of inhibitors, namely, PPMP, a synthetic inhibitor of glucosylceramide synthase [26] and NB-DNJ, an N-alkylated imino sugar that blocks the activity of ceramide-specific glucosyltransferase which catalyzes the formation of glucosylceramide [27], both of which inhibit the conversion of ceramide to glucosylceramide. Indeed, the contents of the C18- and C24-ceramides were significantly augmented in the gastric mucosa when these inhibitors were injected

concomitantly with acetic acid. On the other hand, the acetic acid-induced tissue damage was attenuated with a decrease in the number of apoptotic cells under this condition, suggesting that inhibition of the synthesis of glucosylceramide, a precursor for neutral glycosphingolipids and gangliosides, effectively inhibits ulcer formation.

In the group of acetic acid-induced ulcer, while the glucosylceramide was not increased, the GM3 was remarkably accumulated as compared with the control group, suggesting that ceramide seems to be rapidly metabolized to ganglioside GM3 without accumulating intermediate metabolite such as glucosylceramide. On the other hand, in the group of acetic acid-induced ulcer treated with glucosylceramide synthesis inhibitors, the levels of both glucosylceramide and GM3 were not restored to the control level because glucosylceramide synthesis inhibitors could attenuate the pathway upstream of the glucosylceramide.

In the present study, we examined only the glucosylceramide pathway, and not the other pathways such as the sphingomyelin pathway. According to previous reports, GD3, a downstream metabolite of ceramide, is a key signaling intermediate leading to apoptosis [28], and the recently characterized trafficking of ganglioside GD3 to the mitochondria has revealed a novel function of this lipid as a death effector [29]; thus, the glucosylceramide pathway would be the main pathway, which is co-localized with the other pathways such as the sphingomyelin pathway.

Glucosylceramide synthase is a constitutively expressed type III integral membrane protein on the cytosolic side of the *cis/medial* Golgi membrane [30]. After its translocation to the Golgi lumen by an as yet undefined signaling mechanism, glucosylceramide is further metabolized to higher glycosphingolipids, including GM3 and GD3 gangliosides [11, 31]. It has been suggested previously that glycosylation of ceramide can protect cells from cancer drug-induced apoptosis. Accumulation of glucosylceramide was observed in multidrug-resistant tumor cells [32], and overexpression of glucosylceramide synthase in MCF-7 breast cancer cells conferred resistance to adriamycin and TNF-α [33]. These findings would support the idea that glycosylation of ceramide rather attenuates its capacity to act as a second messenger in apoptosis, although recently, it has been suggested that the natural ceramide species accumulating during the execution phase of apoptosis are not converted by glucosylceramide synthase to glucosylceramide, because this pool of ceramide is topologically segregated from glucosylceramide synthase [11]. In any event, the glucosylceramide formation *per se* does not appear to be a potentially toxic mediator in the acetic acid-induced gastric damage.

In addition to their role in the regulation of apoptosis, ceramides also provide the carbon backbone for the synthesis of complex glycosphingolipids within the Golgi network [34]. Inhibitors of glycosphingolipid biosynthesis have been used successfully as therapeutic agents for glycosphingolipid lysosomal storage diseases [35]. Healthy mice treated with NB-DNJ exhibited 70 % peripheral glycosphingolipid depletion [36], and clinical trials have shown the efficacy of these agents in patients with type 1 Gaucher's disease [37]. In addition, recently, ganglioside GD3 (GD3), a sialic acid-containing glycosphingolipid, has attracted considerable attention due to its emerging role as an effector of cell death by activating the mitochondrial-dependent apoptosis through sequential membrane permeability transition induction, cytochrome c release, and caspase activation [38]. De Maria et al. [39] showed that GD3 ganglioside mediates the propagation of CD95 (Fas)-generated apoptotic signals in hematopoietic cells, and that the pharmacological inhibition of GD3 synthesis and exposure to GD3 synthase antisense oligonucleotides prevented CD95-induced apoptosis. Another group recently demonstrated that the inhibition of glucosylceramide synthase, which blunted TNF-stimulated GD3 levels, abolished TNF-mediated apoptosis in human colon cancer cells [40], and also that *d-threo*-PDMP, an inhibitor of glucosylceramide synthase, blocked the TNF-α-induced translocation of GD3 to the mitochondria, thereby preserving its predominant localization at the cell surface in rat hepatocytes [41]. Since we previously demonstrated that an antibody against TNF-α significantly inhibited ulcer formation in the PMA-induced gastric ulcer model [17], TNF-α may also be involved in the process of acetic acid-induced ulcer formation. These previous reports suggesting that GD3 may play a significant role in TNF-α-mediated apoptosis are in close concordance with our present data indicating that inhibitors of glucosylceramide synthase successfully prevented the apoptosis and ulcer formation induced by acetic acid in spite of the significant accumulation of ceramide content observed in the gastric tissues.

Acknowledgments This study was supported by a Grant-in-Aid for Scientific Research (B) from the Japan Society for the Promotion of Science (22300169, to H.S.), Grant-in-Aid for challenging Exploratory Research (24659103, to H.S.), a grant from the National Defense Medical College (to S.M.), a Research Fund of Mitsukoshi Health and Welfare Foundation (to H.S.), and a grant from the Smoking Research Foundation (to H.S.).

Conflict of interest None.

References

1. Konturek PC, Brzozowski T, Konturek SJ, et al. Apoptosis in gastric mucosa with stress-induced gastric ulcers. *J Physiol Pharmacol.* 1999;50:211–225.
2. Suzuki H, Ishii H. Role of apoptosis in *Helicobacter pylori*-associated gastric mucosal injury. *J Gastroenterol Hepatol.* 2000;15:D46–D54.

3. Suzuki H, Hibi T, Marshall BJ. *Helicobacter pylori*: present status and future prospects in Japan. *J Gastroenterol.* 2007;42: 1–15.
4. Suzuki H, Marshall BJ, Hibi T. Overview: *Helicobacter pylori* and extragastric disease. *Int J Hematol.* 2006;84:291–300.
5. Suzuki H, Iwasaki E, Hibi T. *Helicobacter pylori* and gastric cancer. *Gastric Cancer.* 2009;12:79–87.
6. Leung WK, To KF, Chan FK, Lee TL, Chung SC, Sung JJ. Interaction of *Helicobacter pylori* eradication and non-steroidal anti-inflammatory drugs on gastric epithelial apoptosis and proliferation: implications on ulcerogenesis. *Aliment Pharmacol Ther.* 2000;14:879–885.
7. Nagata H, Akiba Y, Suzuki H, Okano H, Hibi T. Expression of Musashi-1 in the rat stomach and changes during mucosal injury and restitution. *FEBS Lett.* 2006;580:27–33.
8. Liu ES, Cho CH. Relationship between ethanol-induced gastritis and gastric ulcer formation in rats. *Digestion.* 2000;62:232–239.
9. Hakomori S, Igarashi Y. Functional role of glycosphingolipids in cell recognition and signaling. *J Biochem (Tokyo).* 1995;118: 1091–1103.
10. Hannun YA. Functions of ceramide in coordinating cellular responses to stress. *Science.* 1996;274:1855–1859.
11. Tepper AD, Diks SH, van Blitterswijk WJ, Borst J. Glucosylceramide synthase does not attenuate the ceramide pool accumulating during apoptosis induced by CD95 or anti-cancer regimens. *J Biol Chem.* 2000;275:34810–34817.
12. Obeid LM, Linardic CM, Karolak LA, Hannun YA. Programmed cell death induced by ceramide. *Science.* 1993;259:1769–1771.
13. Dbaibo GS, Obeid LM, Hannun YA. Tumor necrosis factor-α (TNF-α) signal transduction through ceramide. Dissociation of growth inhibitory effects of TNF-α from activation of nuclear factor-kappa B. *J Biol Chem.* 1993;268:17762–17766.
14. Kolesnick R, Golde DW. The sphingomyelin pathway in tumor necrosis factor and interleukin-1 signaling. *Cell.* 1994;77: 325–328.
15. Kim MY, Linardic C, Obeid L, Hannun Y. Identification of sphingomyelin turnover as an effector mechanism for the action of tumor necrosis factor α and γ-interferon. Specific role in cell differentiation. *J Biol Chem.* 1991;266:484–489.
16. Cifone MG, De Maria R, Roncaioli P, et al. Apoptotic signaling through CD95 (Fas/Apo-1) activates an acidic sphingomyelinase. *J Exp Med.* 1994;180:1547–1552.
17. Takeuchi T, Miura S, Wang L, et al. Nuclear factor-kappa B and TNF-α mediate gastric ulceration induced by phorbol myristate acetate. *Dig Dis Sci.* 2002;47:2070–2078.
18. Uehara K, Miura S, Takeuchi T, et al. Significant role of ceramide pathway in experimental gastric ulcer formation in rats. *J Pharmacol Exp Ther.* 2003;305:232–239.
19. Koltun E, Richards S, Chan V, et al. Discovery of a new class of glucosylceramide synthase inhibitors. *Bioorg Med Chem Lett.* 2011;21:6773–6777.
20. Shayman JA, Lee L, Abe A, Shu L. Inhibitors of glucosylceramide synthase. *Methods Enzymol.* 2000;311:373–387.
21. Platt FM, Neises GR, Karlsson GB, Dwek RA, Butters TD. N-butyldeoxygalactonojirimycin inhibits glycolipid biosynthesis but does not affect N-linked oligosaccharide processing. *J Biol Chem.* 1994;269:27108–27114.
22. Okabe S, Pfeiffer CJ. Chronicity of acetic acid ulcer in the rat stomach. *Am J Dig Dis.* 1972;17:619–629.
23. Wang E, Norred WP, Bacon CW, Riley RT, Merrill AH Jr. Inhibition of sphingolipid biosynthesis by fumonisins. Implications for diseases associated with Fusarium moniliforme. *J Biol Chem.* 1991;266:14486–14490.
24. Berg H, Magard M, Johansson G, Mathiasson L. Development of a supercritical fluid extraction method for determination of lipid classes and total fat in meats and its comparison with conventional methods. *J Chromatogr A.* 1997;785:345–352.
25. Merrill AH Jr, van Echten G, Wang E, Sandhoff K. Fumonisin B1 inhibits sphingosine (sphinganine) N-acyltransferase and de novo sphingolipid biosynthesis in cultured neurons in situ. *J Biol Chem.* 1993;268:27299–27306.
26. Maurer BJ, Melton L, Billups C, Cabot MC, Reynolds CP. Synergistic cytotoxicity in solid tumor cell lines between N-(4-hydroxyphenyl)retinamide and modulators of ceramide metabolism. *J Natl Cancer Inst.* 2000;92:1897–1909.
27. Svensson M, Frendeus B, Butters T, Platt F, Dwek R, Svanborg C. Glycolipid depletion in antimicrobial therapy. *Mol Microbiol.* 2003;47:453–461.
28. Lovat PE, Corazzari M, Di Sano F, Piacentini M, Redfern CP. The role of gangliosides in fenretinide-induced apoptosis of neuroblastoma. *Cancer Lett.* 2005;228:105–110.
29. Morales A, Colell A, Mari M, Garcia-Ruiz C, Fernandez-Checa JC. Glycosphingolipids and mitochondria: role in apoptosis and disease. *Glycoconj J.* 2004;20:579–588.
30. Jeckel D, Karrenbauer A, Burger KN, van Meer G, Wieland F. Glucosylceramide is synthesized at the cytosolic surface of various Golgi subfractions. *J Cell Biol.* 1992;117:259–267.
31. Ichikawa S, Hirabayashi Y. Glucosylceramide synthase and glycosphingolipid synthesis. *Trends Cell Biol.* 1998;8:198–202.
32. Lavie Y, Cao H, Bursten SL, Giuliano AE, Cabot MC. Accumulation of glucosylceramides in multidrug-resistant cancer cells. *J Biol Chem.* 1996;271:19530–19536.
33. Liu YY, Han TY, Giuliano AE, Ichikawa S, Hirabayashi Y, Cabot MC. Glycosylation of ceramide potentiates cellular resistance to tumor necrosis factor-α-induced apoptosis. *Exp Cell Res.* 1999;252:464–470.
34. Kolter T, Proia RL, Sandhoff K. Combinatorial ganglioside biosynthesis. *J Biol Chem.* 2002;277:25859–25862.
35. Platt FM, Neises GR, Reinkensmeier G, et al. Prevention of lysosomal storage in Tay-Sachs mice treated with N-butyldeoxynojirimycin. *Science.* 1997;276:428–431.
36. Platt FM, Reinkensmeier G, Dwek RA, Butters TD. Extensive glycosphingolipid depletion in the liver and lymphoid organs of mice treated with N-butyldeoxynojirimycin. *J Biol Chem.* 1997;272:19365–19372.
37. Cox T, Lachmann R, Hollak C, et al. Novel oral treatment of Gaucher's disease with N-butyldeoxynojirimycin (OGT 918) to decrease substrate biosynthesis. *Lancet.* 2000;355:1481–1485.
38. Garcia-Ruiz C, Colell A, Paris R, Fernandez-Checa JC. Direct interaction of GD3 ganglioside with mitochondria generates reactive oxygen species followed by mitochondrial permeability transition, cytochrome c release, and caspase activation. *FASEB J.* 2000;14:847–858.
39. De Maria R, Lenti L, Malisan F, et al. Requirement for GD3 ganglioside in CD95- and ceramide-induced apoptosis. *Science.* 1997;277:1652–1655.
40. Colell A, Morales A, Fernandez-Checa JC, Garcia-Ruiz C. Ceramide generated by acidic sphingomyelinase contributes to tumor necrosis factor-α-mediated apoptosis in human colon HT-29 cells through glycosphingolipids formation. Possible role of ganglioside GD3. *FEBS Lett.* 2002;526:135–141.
41. Garcia-Ruiz C, Colell A, Morales A, Calvo M, Enrich C, Fernandez-Checa JC. Trafficking of ganglioside GD3 to mitochondria by tumor necrosis factor-α. *J Biol Chem.* 2002;277: 36443–36448.

Biochemical and Biophysical Research Communications 426 (2012) 33–37

Contents lists available at SciVerse ScienceDirect

Biochemical and Biophysical Research Communications

journal homepage: www.elsevier.com/locate/ybbrc

Development of a novel microRNA promoter microarray for ChIP-on-chip assay to identify epigenetically regulated microRNAs

Yoshimasa Saito [a,b], Hidekazu Suzuki [a,*], Toshiki Taya [c], Masafumi Nishizawa [d], Hitoshi Tsugawa [a], Juntaro Matsuzaki [a], Kenro Hirata [a], Hidetsugu Saito [a,b], Toshifumi Hibi [a]

[a] Division of Gastroenterology and Hepatology, Department of Internal Medicine, Keio University School of Medicine, 35 Shinanomachi, Shinjuku-ku, Tokyo 160-8582, Japan
[b] Division of Pharmacotherapeutics, Keio University Faculty of Pharmacy, 1-5-30 Shibakoen, Minato-ku, Tokyo 105-8512, Japan
[c] Agilent Technologies Japan Ltd., 9-1, Takakura-cho, Hachioji-shi, Tokyo, 192-8510, Japan
[d] Department of Microbiology and Immunology, Keio University School of Medicine, 35 Shinanomachi, Shinjuku-ku, Tokyo 160-8582, Japan

ARTICLE INFO

Article history:
Received 3 August 2012
Available online 11 August 2012

Keywords:
MicroRNA
ChIP-on-chip
Epigenetics
Histone modification
miR-9
Gastric cancer
Epigenetic therapy

ABSTRACT

To gain a global view of epigenetic alterations around microRNA (miRNA) promoter regions, and to identify epigenetically regulated miRNAs, we developed a novel miRNA promoter microarray for chromatin immunoprecipitation (ChIP)-on-chip assay. We designed a custom oligo microarray covering regions spanning −10 to +2.5 kb of precursor miRNAs in the human genome. This microarray covers 541 miRNAs, each of which is covered by approximately 100 probes (60-mer) over its 12.5-kb genomic position, that includes predicted transcription start sites. Using this custom-made miRNA promoter microarray, we successfully performed ChIP-on-chip assay to identify miRNAs regulated by histone modification. Fifty-three miRNAs (9.8%) showed increased levels of both histone H3 acetylation and histone H3-K4 methylation in AGS gastric cancer cells treated with the DNA-methylation inhibitor 5-aza-2′-deoxycytidine and the histone deacetylase inhibitor 4-phenylbutyric acid. One of these miRNAs, *miR-9*, is downregulated in gastric cancer tissues and is activated by chromatin-modifying drugs, suggesting that it may be a potential target for epigenetic therapy of gastric cancer.

1. Introduction

MicroRNAs (miRNAs) are ~22 nucleotide (nt) non-coding RNAs that can post-transcriptionally downregulate the expression of various target genes. Currently, ~1500 human miRNAs have been identified in the human genome, each of which potentially controls hundreds of target genes. In animals, miRNA genes are generally transcribed by RNA polymerase II (pol II) to form primary transcripts (pri-miRNAs). Pol II-transcribed pri-miRNAs are capped with 7-methylguanosine and are polyadenylated. The nuclear RNase III enzyme Drosha and its co-factor DGCR8 process pri-miRNAs into ~60-nt precursor miRNAs (pre-miRNAs), which form an imperfect stem-loop structure. Pre-miRNAs are transported into the cytoplasm by exportin 5 and are subsequently cleaved by Dicer into mature miRNAs, which are then loaded into the RNA-induced silencing complex (RISC). The miRNA/RISC complex downregulates specific gene products by translational repression via binding to partially complementary sequences in the 3′-untranslated regions of the target mRNAs or by directing mRNA degradation via binding to perfectly complementary sequences.

MircoRNAs are expressed in a tissue-specific manner and play important roles in cell proliferation, apoptosis, and differentiation during mammalian development [1]. Links between miRNAs and the development and progression of human malignancies, including gastric cancer, are becoming increasingly apparent [2,3]. Because miRNAs can have large-scale effects through regulation of a variety of target genes during carcinogenesis, understanding the regulatory mechanisms controlling miRNA expression is important. Epigenetic alterations such as DNA methylation and histone modification play critical roles in chromatin remodeling and regulation of gene expression in mammalian development and human diseases, including cancer. We have recently reported that some miRNAs are regulated by epigenetic alterations at their CpG island promoters. Epigenetic treatment with chromatin-modifying drugs such as the DNA-demethylating agent 5-aza-2′-deoxycytidine (5-Aza-CdR) and the histone deacetylase (HDAC) inhibitor 4-phenylbutyric acid (PBA) can reactivate some important tumor suppressor miRNAs, and this may be a novel therapeutic approach for human cancers [4–7]. To gain a global view of epigenetic alterations around miRNA promoter regions and to

Abbreviations: miRNA, microRNA; ChIP, chromatin immunoprecipitation; 5-Aza-CdR, 5-aza-2′-deoxycytidine; HDAC, histone deacetylase; PBA, 4-phenylbutyric acid.

* Corresponding author. Fax: +81 3 5363 3967.
E-mail address: hsuzuki@a6.keio.jp (H. Suzuki).

0006-291X/$ - see front matter © 2012 Elsevier Inc. All rights reserved.
http://dx.doi.org/10.1016/j.bbrc.2012.08.012

identify epigenetically regulated miRNAs, we developed a novel miRNA promoter microarray for chromatin immunoprecipitation (ChIP)-on-chip assay and used it to identify candidate miRNAs regulated by epigenetic mechanisms in human gastric cancer cells.

2. Materials and methods

2.1. MicroRNA promoter microarray

As shown in Fig. 1, we designed a custom oligo microarray covering regions −10 to +2.5 kb surrounding the genomic positions of pre-miRNAs in the human genome (NCBI36/hg18). Briefly, we first downloaded genomic coordinates of pre-miRNAs from the Manchester (previously Sanger) miRBase v10.1. The set of genomic coordinates at the 5′ end of the pre-miRNAs was positioned at zero, and *in silico* pre-designed probes were searched to fit a 4 × 44 K microarray from the high-definition ChIP probe database in eArray provided by Agilent Technologies (Tokyo, Japan). During the probe search, the Tm filter was applied and no homology filter was applied. This microarray covers 541 miRNAs, and each miRNA, spanning an estimated 12.5 kb of genomic sequence (including predicted transcription start sites (TSSs)), is covered by approximately 100 probes (60-mer).

2.2. Cell line and epigenetic treatment

The human gastric cancer cell line AGS was obtained from the American Type Culture Collection (Rockville, MD). Cells were cultured in RPMI1640 medium supplemented with 10% fetal bovine serum. They were seeded at 1×10^5 cells per 100 mm dish 24 h before treatment with 5-Aza-CdR (3 μM, Sigma–Aldrich, St. Louis, MO) and PBA (3 mM, Sigma–Aldrich). After 24 h, 5-Aza-CdR was removed, while the cells were continuously exposed to PBA for 96 h.

2.3. ChIP-on-chip assay

The ChIP assay was performed as described previously [4] using 10 μl of anti-dimethylated histone H3-K4 (Upstate Biochemistry, Lake Placid, NY) and 10 μl of anti-acetylated histone H3 antibodies (Upstate Biochemistry). After ChIP assay, immunoprecipitated DNA was amplified and labeled using Agilent genomic DNA labeling kit

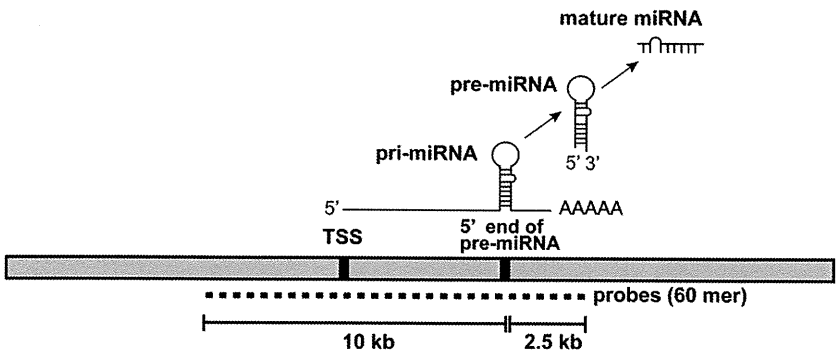

Fig. 1. A design of a custom oligo microarray covering from −10 to +2.5 kb surrounding the genomic positions of pre-miRNAs in the human genome. This microarray covers 541 miRNAs with 125 base spacing between the probes on average, and each miRNA is covered with approximately 100 probes (60-mer) on its 12.5-kb genomic position that includes predicted TSSs.

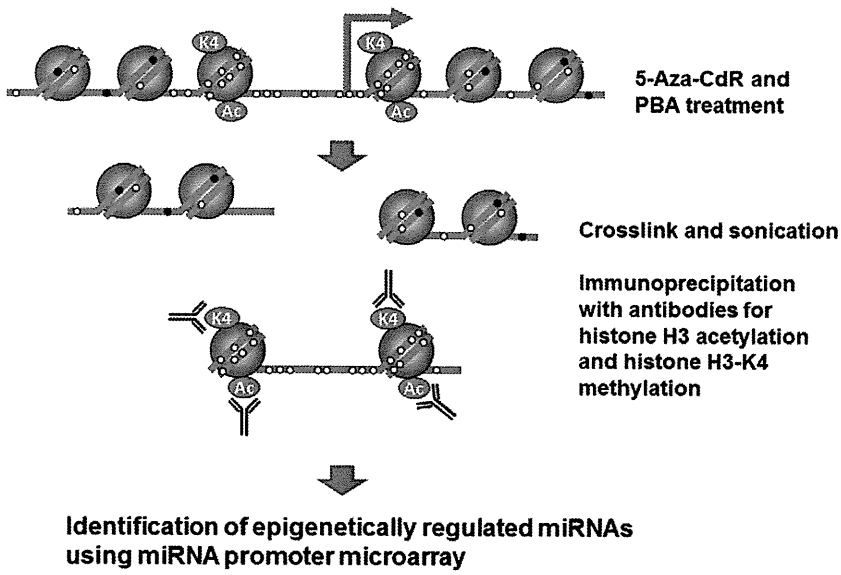

Fig. 2. A scheme of the experimental procedure for ChIP-on-chip assay with miRNA promoter microarray. AGS cells were treated with the DNA-methylation inhibitor 5-Aza-CdR and the HDAC inhibitor PBA. After crosslinking and sonication, chromatin was immunoprecipitated using antibodies for histone H3 acetylation and histone H3-K4 methylation, and immunoprecipitated DNA was hybridized on the miRNA promoter microarray. Open circle, unmethylated DNA; filled circle, methylated DNA; Ac, histone H3 acetylation; K4, histone H3-K4 methylation.